EXPERIMENTAL INVESTIGATION OF FRICTION FACTOR AND HEAT TRANSFER FOR SINGLE PHASE WATER FLOW IN STAINLESS STEEL AND NICKEL MICRO-TUBES

By

QIAN LI

Bachelor of Science in Electromechanical Engineering
University of Macau
Macau, China
2010

Submitted to the Faculty of the
Graduate College of the
Oklahoma State University
in partial fulfillment of
the requirements for
the Degree of
MASTER OF SCIENCE
July, 2012

EXPERIMENTAL INVESTIGATION OF

FRICTION FACTOR AND HEAT TRANSFER

FOR SINGLE PHASE WATER FLOWIN STAINLESS

STEEL AND NICKEL MICRO-TUBES

Thesis Approved:

Dr. Afshin J. Ghajar

Thesis Adviser

Dr. Frank W. Chambers

Dr. Khaled A. Sallam

Dr. Sheryl A. Tucker

Dean of the GraduateCollege

TABLE OF CONTENTS

LIST OF TABLES

LIST OF FIGURES

Figure Page

NOMENCLATURE

Symbol	Description	Unit
A	Area	m^2
D	Tube inner diameter	m
D_h	Hydraulic diameter	m
$D_{h,cf}$	Constricted hydraulic diameter	m
E_r	Error	
f	Friction factor	dimensionless
L	Tube length	m
$\dot{m}$	Mass flow rate	kg/s
Nu	Nusselt number	dimensionless
Δp	Pressure drop	Pa
Pr	Prandtl number	dimensionless
$\dot{Q}$	Heat transfer rate	J/s
$\dot{q}_i''$	Heat flux	W/m^2
Re	Reynolds number	dimensionless
V	Velocity	m/s
Greek Symbols		
ε	Roughness	m
ε_{FP}	Roughness base on constricted parameters	m
ρ	Density	kg/m^3
μ	Absolute viscosity	$Pa \cdot s$

CHAPTER I

INTRODUCTION

In recent years with the advent of the fabrication technology micro tubes can be easily made. Micro tubes are widely used in heat exchanger design to get larger surface area per unit volume, higher heat transfer coefficient, and lower thermal resistance. The studies of micro-tubes' heat transfer behavior became important to assist this kind of heat flux devices cooling devise design.

The normal size tube's heat transfer coefficient can be well predicted by the conventional forced convection heat transfer correlations. However, they have not been verified to work well for predicting the heat transfer coefficient inside the so-called micro tubes. Many researchers already have done some work on the single-phase forced convection heat transfer in micro-tubes. Their results are significantly different from each other. Some of the researchers have found that the friction factors to be below the classical laminar region theory. Meanwhile, some have reported that friction factor correlations for conventional-sized tubes to be applicable for mini- and micro-tubes. However, many recent experiments on small-sized tubes and channels have observed higher friction factors than the correlations for conventional-sized tubes and channels. Their results have been list in Table 2 and Table 7.Due to the difference of the results, it's very necessary to do more research on the investigation of single phase flow in micro-tubes. The results from previous works are different, but it can be clearly seen that the tube diameter and

roughness plays one of the most crucial roles in the friction factor and heat transfer for single phase flow in micro-tubes. The sensitivity of the instruments used in the measurement of pressure drop and temperature also directly affects the final results.

Besides the studying of heat transfer coefficient value in a certain flow region, the studying of flow region change such as the start and end of transition region has become another important topic for micro-tube heat transfer recently. This topic has been initially discussed by Ghajar et al. (2010) and Tam et al. (2011). Their results showed that the start and the end Reynolds number for transition region have been affected by the tube's diameter and roughness. Their work gives us a new way to look at fluid flow inside the micro-tubes. In this research the transition region of single phase flow in micro-tubes will be discussed again.

In this research 7 tubes has been tested. They are 4 stainless steel tubes with diameter 1600, 1000, 762 and 560 μm and 3 Nickel tubes with diameter 1016, 762, 508 μm . These tubes covered a wide range of diameter and roughness. A stable and verified experimental set up has been established. A systematic experimental methodology has been developed and verified for friction factor and heat transfer measurements. The testing Reynolds number range is from 700 to 8000. The major objectives of this study are to accurately measure the friction factor and heat transfer for different tubes with different roughness and diameter under different heating conditions from laminar to turbulent region and explore how the roughness, diameter and heating affect the start and end of the transition region in these micro-tubes.

In this thesis, after introduction a brief literature review will appear in chapter 2. The literature review was divided into two parts: friction factor and heat transfer. Chapter 3 will discuss the experimental set up and methodology in detail. The experimental results will be discussed in Chapter 4. The final conclusions will be given in Chapter 5.

CHAPTER II

REVIEW OF LITERATURE

2.1-Pressure Drop in Micro-channels/tubes

Numerous experiments about micro scale fluid flow have been conducted by different researchers within this decade. One major area of research in fluid flow in micro-channels is the friction factor, or the pressure drop. However, controversial results are found among different experiments, including a large discrepancy in the transitional Reynolds number, the effect of roughness on pressure drop, and the applicability of the conventional equations for the prediction of friction factor in micro-channels.

Mala and Li (1999) conducted experiments on the flow characteristics of water in micro-tubes with diameter ranging from 50 to 254μm. The materials for the micro-tubes were stainless steel and fused silica. They found the experimental data fitted roughly to the result predicted by the conventional theory only at small Reynolds numbers (< 2500). They reported higher friction factor in micro-tubes than that predicted by conventional theory. Early laminar-turbulent transition at Reynolds number ranging from 300-900 was also found in their experiment and they attributed this phenomenon to the roughness.

Qu and Mudawar (2002) studied the pressure drop and heat transfer in a micro-channel heat sink numerically and experimentally. The dimensions for the rectangular tube in heat sink was 231 μm wide and 713 μm deep. They choose different Reynolds number range for different heat flux. In the numerical analysis, they choose a unit cell containing a micro-channel and surrounding solid and then extended the results into the whole part according to the symmetry. They reported a good agreement between the experimental results and numerical values. Also, the conventional Navier-Stokes equations could be used for the prediction of the experimental data with good accuracy. Moreover, no early laminar-turbulent transition was found in their experiments.

Yin et al. (2002) performed pressure drop experiments in a micro-channel heat exchanger. The port diameter for the micro-channel was 0.787 mm with a length of 815mm; the working fluid was R774. They concluded that the typical friction factor correlation can be applied well to predict the major and minor losses in micro-channels.

Celata et al. (2002) investigated the friction factor for R-114 in a micro-tube with 130 μm diameter. The Reynolds number ranged from 1000 to 8000. They reported a good agreement with the classical theory for the laminar flow when the Reynolds number was below 585. For the Reynolds number between 585 and 1880, it is also laminar flow but the friction factor in this range is higher than the predicted value and the authors attributed this deviation to the roughness. The transitional flow occurred when the Reynolds number was between 1880 and 2480. Above 2480, the flow fell into the turbulent region and the friction factor fit well with the classical theory.

Brutin and Tadrist (2003) examined the friction factor of the laminar flow of water through fused silica tubes with diameters ranging from 50 to 530μm. They reported a deviation from the Stokes flow theory and also a higher friction factor compared with classical theory. They also found this kind of deviation decrease with the increase of diameter. No detailed explanations are given to such a conclusion but they attribute this partly to the ionic composition of the fluid.

Li et al. (2003) performed experimental study on the flow characteristics of deionized water through circular micro-tubes which were made of three different materials: glass, silica, and stainless steel. The glass tubes with diameter ranging from 79.9-166.3μm and the silica tubes with diameter ranging from 100.25-205.3μm can be treated as smooth tubes. The stainless steel tubes with diameter ranging from 128.76-179.8μm were treated as rough tubes. They concluded that the conventional theory for laminar flow can be applied to the smooth micro-tubes. However, for the turbulent flow, the product of friction factor and Reynolds number (f*Re) were slightly larger than that predicted by using conventional theory. As for the laminar-turbulent transition, no early transition was found for most tubes except for the stainless steel tubes with diameter of 128.76 μm. But the conclusion for early transition may not be asserted until more experiments are performed for similar tubes.

Kandlikar et al. (2003) investigated the effect of roughness on pressure drop in microtubes. The roughness was changed by etching the tubes with different acids. They observed that for larger tubes (1067μm), the effect of roughness is negligible. For smaller tubes (620 μm), increases in roughness (from 998nm to 2201nm) resulted in higher pressure drop accompanied by early transition.

Cui et al. (2004) studied the flow behavior for distilled water, iso-propanol and carbon tetra-chloride under high pressures in micro-tubes ranging from 10 μm to 3 μm. The Reynolds number in their experiments ranged from 0.1- 24. The results from the experiment were compared with the conventional Hagen-Poiseuille (HP) law and some deviations were found. For the 10 μm tubes, the flow behaviors of isopropanol and carbon tetra-chloride were different from the HP law, but water did not show similar behavior. The normalized friction coefficient for iso-propanol and carbon tetra-chloride increased with the pressure but for water, the variation for this coefficient was slight. They also introduced a revised HP equation which fitted well with their experimental data.

Asako et al. (2005) studied the product of friction factor and Reynolds number of air flow in micro-tube with 150 μm diameter and 5 nm average roughness. The observed f*Re differ from the incompressible value which is 64. Furthermore, they reported the value for f*Re is a function of Mach number and correlations were introduced in their paper.

Celeta et al. (2006a) investigated the influence of channel wall roughness and of wall hydrophobicity on adiabatic flow in circular micro-channels ranging from 70 to 326 μm. The flow behavior for water in smooth tubes down to 30 μm was also ascertained. The results they got agreed with the classical Hagen-Poiseuille law within experimental uncertainty. They also attributed the deviation to the circular geometry rather than the roughness.

Celata et al. (2006b) investigated the compressible flow of helium flowing through fused silica micro-tubes ranging from 30 to 254 μm. They made conclusion that the "quasi-compressible"

equations for the friction factor can be used for the prediction of the flow character in micro-tubes. Moreover, the density change of fluid flow was also applied to their experimental data.

Morini et al. (2006) investigated the flow characteristics of nitrogen flowing through stainless steel tubes with diameters of 762, 508, 254 and 127 μm. The friction factor they obtained from their experiment was compared with three conventional equations used to predict the friction factor. They made conclusion that the friction factor can be well predicted by using one of three equations obtained before. They also asserted that no early transition was found in their experiment but the dependence of critical Reynolds number on the relative roughness of the tube seemed to be confirmed.

Steinke and Kandlikar (2006) examined the friction factor for degassed water flowing through silica rectangular micro-tube with a width of 200 μm, a depth of 250 μm, and a length of 10 mm. The Reynolds number in their experiment ranged from 14 to 789. Their experiments covered both single-phase and two-phase flows but we just concentrate on the single-phase part. They reported a rough agreement with the conventional theory after performing data correction. They also paid extra attention to the geometry of the micro-tubes and concluded the geometry would exert great influence on the flow characteristics.

Hwang and Kim (2006) studied the pressure drop of R-134a flowing through stainless steel micro-tubes with diameters of 0.244, 0.430, and 0.792 μm. They investigated the single-phase pressure drop and also the two-phase pressure drop. They reported a good agreement with the classical theory within an absolute average deviation of 8.9% for the single phase flow.

Moreover, no early transition was found in their experiment. The effect of roughness was not discussed in their paper but the roughness of the tubes was given.

Rands et al. (2006) conducted study on the characterization of laminar-turbulent transition for water flow in micro-tubes ranging from 16.6 μm to 32.2 μm. They reported macro-scale behavior in their experiments and the laminar-turbulent transition occurred at the Reynolds number ranging from 2100-2500. They also found a slight dependency between the critical Reynolds number and the diameters of tubes.

Hrnjak and Tu (2007) examined the pressure drop of R-134a flowing through PVC micro-tubes with hydraulic diameter ranging from 69.5 μm to 304.7 μm. The Reynolds number covered was from 112 to 9180. They reported a good agreement with the conventional theory applied for macro-tubes in laminar region. But for the turbulent region, the friction factor was slightly higher than that predicted by using Churchill's equations for smooth tubes, they attributed such a phenomenon to the roughness and also concluded that so-called "smooth" tubes were difficult to achieve in micro-scale. They also found the importance of the roughness on pressure drop after observing an abnormal result obtained by using the micro-tube with largest roughness. Moreover, they reported a marginal larger value for critical Reynolds number and they explained it as the effect of roughness.

Qi et al. (2007) investigated the single-phase pressure drop and heat transfer characteristics of turbulent liquid nitrogen flow in stainless steel micro-tubes. The diameters for the tubes were 1.931, 1.042, 0.834, and 0.531 mm; the Reynolds number in their experiment ranged from 10000-

90000. After comparing their result with the conventional theory, they concluded that the friction factor in micro-tubes is higher than that predicted by conventional theory for macro-scale tubes and they attributed this phenomenon to the inner roughness of the tubes. They also concluded that the Colebrook correlation can be used for the prediction of friction factor in micro-tubes but some modifications based on the surface roughness are needed.

Ghajar et al. (2010) investigated the friction factor in the transition region for single phase flow in stainless steel micro-tubes ranging from 2080 μm to 690 μm. They paid particular attention the sensitivity of the instruments and the pressure-sensing diaphragms. They found that the decrease in tube diameter actually delayed the transitional region. Furthermore, the friction factor profile was not significantly influenced by the decrease of diameter until reaching around 1300 μm. They also studied the effect of roughness on the pressure drop and made conclusion that the roughness would be important for micro-tubes with small diameters.

Singh (2011) investigated the friction factor of 4 Nickel micro tubes ranging from 1016 to 381 μm. He found that critical Reynolds number of Nickel tube reduced with decrement in diameter. In his thesis, the Nickel tubes' results have been compared with the results from stainless steel and glass tubes, and concluded that there is no roughness effect for low relative roughness (0.005-0.013%).

Tam et al. (2011) investigated the effect of inner surface roughness and heating on friction factor in horizontal micro tubes. In their research work three stainless steel tubes with 750 μm, 1000 μm and 2000 μm inner diameters were tested. The inner surface was etched by acid in order to get

different roughness. The friction factor was measured under both isothermal and heating conditions. The results showed that heating reduced the laminar and transition friction factor and delayed the start of transition and the range of transition Reynolds number was narrower with the increase of surface roughness.

Based on the review above, the important aspects of the previous research, which are (1) test conditions, (2) critical Reynolds number, (3) uncertainty of the experiments, and (4) instruments used, are summarized in Tables 1 to 4, respectively.

Table 1 Summary of Test Conditions

Author (Year)	Re Range	Hydraulic Diameters(μm)	Test Fluid	Micro-tube Material	Surface Roughness
Mala and Li(1999)	0-2500	50-254	deionized water	stainless steel, fused silica	1750nm
Qu and Mudawar (2002)	0-1800	748	distilled water	oxygen-free copper	_
Yin et al. (2002)	0-6000	696-1494	nitrogen	_	5.25, 4.55, 5.2, 4.1 micrometer
Celata et al. (2002)	100-8000	130	R-114	stainless steel 316	3450nm
Brutin and Tadrist (2003)	0-1000	50-500	tap water, distilled water	fused silica	10nm
Li et al. (2003)	500-2500	Glass: 79.9-166.3; silica: 100.25-205.3; ss: 128.76-179.8	de-ionized water	glass, silicon, stainless steel	50nm for glass, 5500 for stainless steel
Kandlikar et al. (2003)	500-3000	SS 620,1032	distilled water	stainless steel	2322nm, 1837nm, 2900nm for 1032μm 2201nm, 1798nm, 998nm for 620μm
Cui et al. (2004)	0-24	3 to 10	distilled water, iso-propanol, carbon-tetrachloride	_	7.12nm
Asako et al. (2005)	_	150	air	fused silica	5nm
Celeta et al. (2006a)	300-	31-300	degassed water	fused silica, glass teflon	200-700nm
Celeta et al. (2006b)	0.8-500	254, 101, 50, 30	He	fused silica	<500nm
Morini et al. (2006)	0-10000	762, 508, 127	nitrogen	stainless steel	_
Steinke and Kandlikar (2006)	14-789	222	degassed water	silica	1500-2500nm
Hwang and Kim (2006)	100-10000	244, 430, 792	R-314a	stainless steel	397, 486, 341
Rands et al. (2006)	300-3400	16.6, 19.7, 26.3, 32.2	water	_	_
Hrnjak and Tu (2007)	100-10000	304.7, 150, 141.1, 104.1, 69.5 (Rectangle)	R-134a	PVC	ε/D =0.16%, 0.3%, 0.35%
Qi et al. (2007)	10000-90000	531, 834, 1042, 1931	liquid nitrogen	stainless steel 304	2310, 1720, 860, 670
Ghajar et al. (2010)	500-10000	1082.8, 1600.2, 1374.1, 1066.8, 838.2, 685.8	distilled water	alloy 304 stainless steel (Small Parts Inc.)	410nm
Singh (2011)	500-10000	1016, 762, 508, 381	water	nickel	51nm
Tam et al. (2011)	800-13000	1000,750	distilled water	stainless steel	ε=3.29μm, 3.45μm, 4.32μm for 1000μm. ε=3.38μm, 4.70μm, 4.86μm for 750μm

Table 2 Summary of Critical Reynolds Number and Related Results

Author (Year)	Critical Reynolds Number	f*Re
Mala and Li (1999)	300-900 for L to T, 1000-1500 turbulent, early transition	larger
Qu and Mudawar (2002)	_	agree
Yin et al. (2002)	1200	agree
Celata et al. (2002)	1880-2480 for 17 degree, 2245-2295 for 33 degree	agree untill 580, then higher
Brutin and Tadrist (2003)	1800-3000	agree for 800-1000, higher for >1000
Li et al. (2003)	around 2200	agree for glass and silica tubes, higher for stainless steel
Kandlikar et al. (2003)	500-3000	_
Cui et al. (2004)	_	higher
Asako et al. (2005)	_	higher
Celeta et al. (2006a)	2000 to 3000	agree
Celeta et al. (2006b)	_	agree
Morini et al. (2006)	1800-2900	agree in laminar range
Steinke and Kandlikar (2006)	300, early transition to turbulent	higher
Hwang and Kim (2006)	slightly less than 2000	agree
Rands et al. (2006)	2100-2500	agree
Hrnjak and Tu (2007)	2190, 3000	higher
Qi et al. (2007)	_	higher
Ghajar et al. (2010)	1500 for 2080μm and delayed with the decrease of diameter, 2500 for 686μm	_
Singh (2011)	1650, 1450, 950, 1850	_
Tam et al. (2011)	2144.2306,2373 for 1000μm with the increase of roughness. 2196, 2296, 2100 for 750μm with the increase of roughness	_

Table 3 Summary of Uncertainty

Author (Year)	Pressure (± %)	Flow (±)	Diameter (±)	Re (±)	f
Mala and Li (1999)	2%	2%	2%	3%	9.20%
Qu and Mudawar (2002)	3.50%	4%	_	_	_
Yin et al. (2002)	0.25%	0.1%	_	_	_
Celata et al. (2002)	_	0.7 to 7%	_	0.1 to 5%	6 to 7%
Brutin and Tadrist (2003)	20Pa	10mg	1.17%-3.2%	_	1.7% to 4.56%
Li et al. (2003)	5%	2%	2%	_	_
Kandlikar et al. (2003)	_	_	_	_	0.7%
Cui et al.	0.30%	_	_	_	_
Asako et al. (2005)	_	1%	200nm	_	_
Celeta et al. (2006a)	_	_	820-6400 nm	_	_
Celeta et al. (2006b)	_	>1%	_	_	19%
Morini et al. (2006)	0.50%	0.60%	2%	3%	10%
Steinke and Kandlikar (2006)	3.00%	0.50%	3%	6.10%	6.50%
Hwang and Kim (2006)	_	_	_	_	4.60%
Rands et al. (2006)	_	_	1000nm	_	_
Hrnjak and Tu (2007)	3.5kPa for absolute and 0.017kPa to 0.43 kPa	0.7% to 2%	_	1% to 2%	4.5% to 6.3%
Qi et al. (2007)	0.3kpa	2%	0.001mm	2.10%	6.30%
Ghajar et al. (2010)	0.4% (worst is 1%)	1.80%	1.43% to 6.51%	_	3%
Singh (2011)	0.4% (worst is 1%)	1.80%	1.43% to 6.51%	_	1.51 to 3%
Tam et al. (2011)	1.0%	_	_	_	5%

Table 4 Summary of Instruments

Author (Year)	Method used to pump fluid	Pressure	Flow	Diameter
Mala and Li (1999)	precision pump (Ruska)	pressure transducers	reading in pump, flow sensors	–
Qu and Mudawar (2002)	gear pump	two absolute pressure transducer at inlet and outlet	two rotameters	–
Yin et al. (2002)	nitrogen gas cylinder	absolute and differential pressure transducers	coriolis-type mass flow meter	wire gauge
Celata et al. (2002)	Piston pump	pressure transducer	flow meters bank	SEM (LEO 1503)
Brutin and Tadrist (2003)	pressurized tank	pressure sensor (Sensym)	mass balance (Satorius)	SEM and ccd camera
Li et al. (2003)	pressurized tank	absolute pressure transducers	weighing mass of fluid	SEM
Kandlikar et al. (2003)	Water pump	Pressure transducer	flow meter	SEM
Cui et al. (2004)	high pressure pump	pressure transducer	_	SEM
Asako et al. (2005)	nitrogen gas cylinder	pressure transducer (Valcom)	flow meter (Kofloc)	Atomic force microscope
Celeta et al. (2006a)	gear pump	pressure transducer and differential manometer	high precision scale balance	SEM (LEO 1503)
Celeta et al. (2006b)	pnewmatic	absolute pressure transducers(Drunk) and differential manometer (Rosemount)	mass flow meter (Bronkhorst EL-Flow)	SEM (LEO 1503)
Morini et al. (2006)	high pressure flask	differential pressure transducer (Validynemodel DP15)	two flow sensors (Bronkhorst EL-Flow)	SEM apparatus (JEOL JSM 5200)
Steinke and Kandlikar (2006)	gear pump (Micropump)	differential pressure transducer (Omega)	flow meter bank	SEM
Hwang and Kim (2006)	two syringe pumps	differential pressure transducer	mass flow meter	SEM
Rands et al. (2006)	high pressure syringe pump	pressure transducer	_	SEM
Hrnjak and Tu (2007)	pump	two Absolute pressure transducers(Setra) and three differential pressure transducers(Setra)	two mass flow meters(Micromotion and Rheotherm), digital balance (Sartorius Model BP6100)	Surface profilometer (Sloan Dektak ST)
Qi et al. (2007)	vacuum pump and nitrogen gas cylinder	two absolute pressure transducer	vortex flow meter	500*microscopy
Ghajar et al. (2010)	pneumatic and hydraulic combination	differential pressure transducer (Validyne model DP15)	two coriolis flow meters (Micro Motion Inc.)	SEM and digital camera
Singh (2011)	pressurized tank	differential pressure transducer (Validyne model DP15)	two coriolis flow meters (Micro Motion Inc.)	SEM and digital camera
Tam et al. (2011)	pressurized tank	differential pressure transducer (Validynemodel DP15)	coriolis flow meters (Micro Motion Inc.)	SEM and digital camera

2.2 Micro-tube Heat Transfer Investigation

For the experiments on heat transfer in micro-tubes, the results are mixed. Owing to the difficulty in conducting experiments on gases, it is observed that most of the gas-flow studies are either numerical or analytical. In this report, the literature survey will be focused on experimental work only.

Celata et al. (2002) investigated an experimental study on the hydraulic characteristics and single-phase thermal behavior of a capillary tube with internal diameter of 130μm, as the Reynolds number varied in the range from 100 up to 8000. Their experiments showed that the transition from laminar to turbulent occurred for Reynolds numbers in the range 1880-2480. In addition, the heat transfer data in laminar and turbulent regimes did not agree well with the correlations for conventional tubes.

Kandlikar et al. (2003) investigated the effect of roughness on heat transfer in micro-tubes. The roughness was changed by etching the tubes with different acids. They observed that for the larger tube (1067 μm), the effect of roughness is negligible. For smaller tube (620 μm) an increase in roughness resulted in enhanced heat transfer. In this research, the results showed that for the same diameter size tubes the higher roughness yielded the higher heat transfer.

Owhaib and Palm (2004) studied the heat transfer characteristics of single-phase forced convection of R134 through single circular tubes with inner diameters of 1.7mm, 1.2mm as well as 0.9mm. T-type thermocouples were used to measure the surface temperature of tubes. The Reynolds number ranged from 1000 to 15000. It was stated that the experimental results were in fair agreement with classical turbulent heat transfer correlations. In the laminar regime, the heat

transfer coefficients (h) were almost identical for all three diameters. However, their experimental results had a very high Nusselt number scattering distribution.

Shen et al. (2005) conducted an experimental study on the single-phase convective heat transfer in a compact heat sink consisting of rectangular micro channels of 300μm widths and 800μm depths. They used deionized water as the working fluid. Their tests were performed in the Reynolds number range of 162-1257. They found that the surface roughness had a great effect on the laminar flow in rough micro channels. For developed flow, the Poiseuille number in the regime of high Reynolds number was higher than the conventional theory predictions and increased with increasing Reynolds number, rather than remaining constant. However, such effect can be neglected for low Reynolds numbers. Their analysis also showed that higher inlet fluid temperature and heating power can provide better overall flow and thermal performance.

Celata et al. (2006c) investigated experimentally the behavior of single-phase flow in micro-tubes using water as the test fluid. Thermally developing flow effects were observed in large diameter tubes while smaller diameter tubes exhibited low Nusselt number values at small Reynolds numbers. They concluded that in high Reynolds number the convective heat absorption of the fluid in the tube is not the dominant force any more, but is counterbalanced by a dissipation term that is unaccounted for.

Muwanga and Hassan (2006) used un-encapsulated thermo chromic liquid crystal to measure the local heat transfer coefficient in a micro channel with 1.0668mm inner diameter and outer

diameter of 1.27mm. Their results indicated that the conventional correlation is adequate for predicting the heat transfer coefficient.

Qi et al. (2007) conducted experimental studies on the single-phase pressure drop and heat transfer characteristics of liquid nitrogen in four micro-tubes with inner diameters of 1.931mm, 1.042mm, 0.834mm as well as 0.531mm. They found that the local heat transfer coefficient of liquid nitrogen flow in the micro-tubes dropped by 12.5% along the tube. The average Nusselt numbers for the micro-tubes are higher than those predicted by the correlations for the conventional channels. They also indicated that the local heat transfer coefficient decreases along the flow direction and also decreases with the increase of the heat flux. They explained that the main reason is that the thermal conductivity of liquid nitrogen is inversely proportional to temperature.

Yang and Lin (2007) investigated heat transfer characteristics of water flow in micro-tubes with inner diameters range from 123μm to 962μm. A non-contact liquid crystal thermograph (LCT) temperature measurement method was used to measure the surface temperature of micro-tubes. They concluded that the conventional heat transfer correlations for laminar and turbulent flow can be well applied for predicting the fully developed heat transfer performance in micro-tubes. The transition from laminar to transition was observed at Reynolds numbers from 2300 to 3000, which agreed well with the conventional tubes. They found that there is no significant size effect for water flow in tubes within this diameter range. Moreover, the laminar thermal entrance length for micro-tubes was observed to be longer than that estimated by the conventional correlations.

Zhigang et al. (2007) investigated quartz micro-tubes with diameter of 45, 92, and 141μm. The tubes were heated by a thin brass wire. The researchers put the heating wire's two ends into a DC ohm meter to measure the resistance of the heating wire. They introduced a correlation of temperature and resistance to calculate the temperature of heating wire and then calculated surface temperature of the testing tube. The results showed that when the Reynolds number exceeded 1000, the heat transfer rate sharply increased and was higher than the predictions by the classical transitional correlations.

Li et al. (2007) placed five T-type TCs on the surface of testing tube. The heating on the tube wall was offered by an electrical DC power supply. The DC power supply could provide a maximum of 100A current. The authors mentioned that it took about 45 min to reach a steady state.

Morini et al. (2010) provided a table of maximum Reynolds number reachable for a fixed pressure drop as a function of the micro-tube dimensions. In their experiments 50-μm K-type thermocouples were used to measure the temperature of micro-tube outside surface. These K-type TCs were glued with cyanacrylate and subsequently fixed with a nonconductive epoxy resin. In this paper, the authors discussed Roughness Effects and concluded: it is important to stress that the correlations presented by Gnielinski are valid for smooth tubes forced convection.

Tam et al. (2012) studied micro tube heat transfer rate by using liquid crystal thermography (LCT) method. In their study, 2 tubes with diameters of 2000 μm and 1000 μm were tested. They concluded that the heat transfer rate measured by LCT method was lower than the heat transfer rate measured by thermocouples.

Based on the above review, the important aspects of the previous research, which are (1) summary of experiments, (2) measurements and uncertainties, (3) effect of roughness and diameter on heat transfer in micro-tubes, are summarized in Tables 5 to 7, respectively.

Table 5: Summary of Heat Transfer Experiments

Author (Year)	Test Fluid	Tube Material	Micro Tube Diameter (μm)	Tube Length (mm)	Re Range	Correlation Compared
Celata et al. (2002)	R114	stainless steel	130	–	100-8000	Gnielinski Dittus-Boelter Hausen Modified Gnielinski
Kandlikar et al. (2003)	water	stainless steel	1032 620	–	500-2600	Shah and London
Owhaib and Palm (2004)	R134a	glass	1700 1200 800	325	1000-17000	Gnielinski Dittus-Boelter Hausen Adams Wu and Little Petukhov Sieder and Tate
Shen et al. (2005)	deionized water	copper	80	50	162-1257	Kandlikar Poiseuille
Celata et al. (2006c)	dematerialized water and degassed	glass	528 325 259 120 50	–	>100	Gnielinski
Muwanga and Hassan (2006)	water	stainless steel	1066.8	–	610-4400	Shah and London
Qi et al. (2007)	liquid nitrogen	stainless steel	19.31 10.42 8.34 5.31	250 250 250 250	10000-90000	Dittus and Boelter and Gnielinski
Yang and Lin (2007)	water	stainless steel	123(Long) 123(Short) 962	140 64 356	100-10000	Yang Gnielinski Yu Adams
Zhigang et al. (2007)	water	quartz glass	45 92 141	41.49 85.23 136.89	100-3000	Shah &Bhatti, Dittus-Boelter, Petukhov
Li et al. (2007)	water	fused silica and Stainless steel	100 75 50 1570 624.4 373	30 300	20-2400	Numerical
Morini et al. (2010)	water FC-72	stainless steel	440 280 146	92.9 88.8 52.8	350-7000	Gnielinski
Tam et al.(2012)	water	stainless steel	2000, 1000	450, 275	700-1500	Gnielinski, Dittus-Boelter

Table 6: Measurements and Uncertainties

Author (Year)	Boundary Condition	Temperature Measurement	Uncertainty		
			T	H	Nu
Celata et al. (2002)	Isothermal	Vapor temperature measured	–	Higher value obtained	Re<1000: 20% Re<2500: 5% Re>2500: 0.5%
Kandlikar et al. (2003)	Iso-flux	type-K thermocouples	–	–	5%
Owhaib and Palm (2004)	Iso-flux	type-T thermocouples	0.2	–	–
Shen et al. (2005)	Iso-flux	type-K thermocouples	1.67%	–	5.93%
Celata et al. (2006c)	Iso-flux	type-K thermocouples	0.1	–	–
Muwanga and Hassan (2006)	Iso-flux	LCT	1.1	–	23.7%
Qi et al. (2007)	Isothermal &Iso-flux	type-T thermocouples	0.1	2.1%	7.8%
Yang and Lin (2007)	Iso-flux	LCT	0.1	−	2%-12%
Zhigang et al. (2007)	Iso-flux	DC ohmmeter	0.2%	–	10.5% for Re<1000, 8.1% for Re>1000
Li et al. (2007)	Iso-flux	Type-T thermocouples	3.12%	4.47%	5.48%
Morini et al.(2010)	Iso-flux	Type-K thermocouples	0.3	–	± 7%
Tam et al.(2012)	Iso-flux	LCT	0.22	22%	22%

Table 7: Effect of Roughness and Diameter on Heat Transfer in Micro-tubes

Authors (Year)	Diameter (μm)	Roughness (μm)	ε/D	Conclusion
Celata et al. (2002)	130	3.42	0.0265	For laminar flow, the experimental results are lower than conventional theory; for turbulent flow, the experimental results are higher than Gnieliski. And agree well with Adams et al. for high inlet temperature.
Kandlikar et al. (2003)	1032 620	2.4, 1.9,and 3.0 for 1032 μm tubes 2.2, 1.8,and 1.0 for 620 μm tubes	0.00225, 0.00178, and 0.00281 for 1032 μm tubes 0.00355, 0.00290, and 0.00161 for 620 μm tubes	The agreement with Shah and London correlation is within the experimental uncertainties.
Owhaib and Palm (2004)	1700 1200 800	–	–	The result shows that the classical correlations were in good agreement with the experiments data.
Shen et al. (2005)	80	–	4-6%	Surface roughness has a great effect on the laminar flow. Poiseuille number for high Re value is higher than conventional theory.
Celata et al. (2006c)	528 325 259 120 50	smooth	–	Heat transfer performance is lower than the conventional value (Nu = 4.36).
Muwanga and Hussan (2006)	1066.8	–	–	Conventional correlation is adequate for predicting the heat transfer coefficient.
Qi et al. (2007)	19.31 10.42 8.34 5.31	0.67 0.86 1.72 2.31	0.000347 0.000825 0.00206 0.00435	Modified Gnielinski correlation can accurately predict the experiments data taking into account the effect of surface roughness. The correlations for micro-tubes overestimate the average Nu number with large deviation.
Yang and Lin (2007)	123.0 220.4 308.3 416.1 763.5 962.0	1.40 1.48 1.34 1.46 1.16 1.40	0.0114 0.00672 0.00435 0.00352 0.00152 0.00146	Agree well with Gnielinski for laminar flow Different from Gnielinske from Re range of 2500 to 3500
Zhigang et al. (2007)	45 92 141	smooth	–	Higher than the classical transitional correlations when Re>1000.
Li et al. (2007)	100 75 50 1570 624.4 373	15,9	0.95% 1.4% 2.4%	At low Re the increase of the wall thickness over hydrodynamic diameter ratio leads to a larger discrepancy of heat transfer results between experimental and conventional results.
Morini et al. (2010)	440 280 146	3 to 6	0.7% to 4%	Gnielinski is validated for high Reynolds number.
Tam et al.(2012)	2000 1000	4.72 3.29	0.00213 0.00329	Gnielinski and Dittus-Boelter validated for turbulent region

CHAPTER III

EXPERIMENTAL SETUP & METHODOLOGY

Effective experimental setup and instrumentation play an important role in reducing the experimental uncertainties and measurement errors. As shown in Chapter II (Review of Literature) there have been wide disparities in the results obtained by the researchers for which accuracy of the data obtained from the setup used can be questioned. This chapter discusses in detail the experimental setup involved in taking the pressure drop and tube surface temperature measurements. The pressure drop data are used for friction factor calculations. Tube surface temperature and input heat measurement data are used for heat transfer rate calculations. The experimental setup consisted of five major parts: (1) fluid delivery system, (2) fluid flow measurement system, (3) test section assembly, (4) DC Power supply and (5) data acquisition system. The setup is fairly simple to operate but at the same time very effective in obtaining the results required. The setup is also very flexible in nature considering the use of different diameters of tubes and testing. Assembly schematic of the experimental set up is shown in Figure 3.1 and details are discussed subsequently. It is an open loop system. Testing fluid leaving the test section is collected in a sealed container and reused for the experiment.

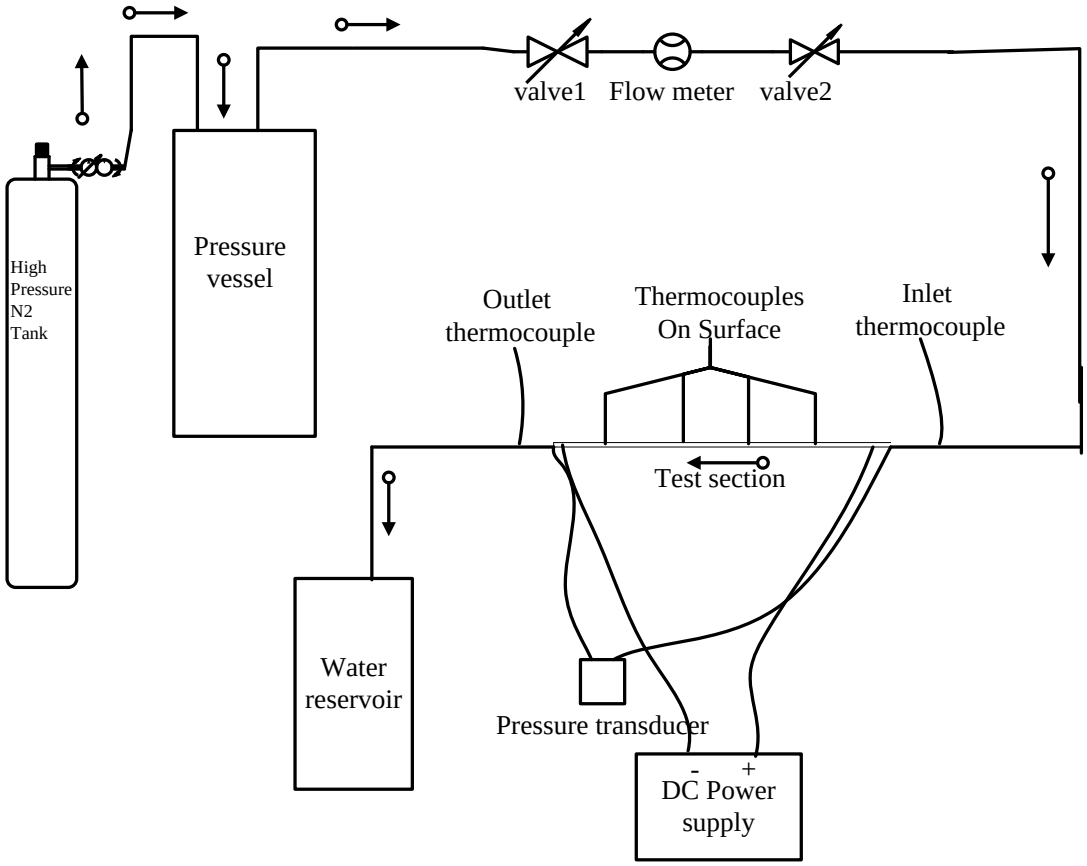

Figure 3.1 Schematic diagram of the experimental setup

3.1 Details of the Experimental Setup

3.1.1- Fluid Delivery System

Fluid delivery system used for this setup was pneumatically pressurized consisting of high pressure nitrogen cylinder (17236 KPa) which gives pressure to water as required in the system. This testing system is an open loop system. After the fluid exiting the setup, it is collected in a sealed container and refilled manually. Nitrogen is forced into a pressure vessel by help of a dual-stage regulator; pressure vessel is of stainless steel containing the distilled water for experiment.

Nitrogen is forced into the pressure vessel from the bottom leading water to push up in a vertical pipe which directs the water flow towards flow measurement assembly before passing through the test section.

Dual stage regulator installed on the pressure tank can deliver pressure up to 250 psi to the stainless steel pressure vessel (Alloy products Model no. 72-05) of capacity 5 Gallon (19 Liters). This pressure vessel works on a maximum pressure of 200 psi and due to this the maximum pressure drop achievable for the test section has a limitation of 200 psi. Water after passing through the pressure vessel flows through a 1/4inch Omegalex PFA chemical tubing leading to the metering valve (Parker N-Series Model 6A-NIL-NE-SS-V) which controls the amount of water flow into flow meter. Metering valve helps in adjusting the flow according to the Reynolds number required for the flow which is not achievable through the dual stage regulator. Flow meter arrangement has two types of mass flow meters. One meter is for high flow rates and the other one is for low flow rates. Specifications are discussed under the heading fluid flow measurement system next. Water after passing through flow meter arrangement again passes through Omegalex PFA chemical tubing exiting the flow meter arrangement and entering the test section assembly and then exiting the whole setup and is collected in a sealed container for reuse.

3.1.2- Fluid Flow Measurement System

Two flow meters were used in this experiment and they were provided by Micro Motion Inc. High flow meter is CMF025 coupled with 1700 transmitter, and designed to measure mass flows ranging from 54 kg/hr (119 lbm/hr) to 2180 kg/hr (4806 lbm/hr) with accuracy of 0.05%. Low flow meter is Micro Motion Model LMF3M, coupled with LFT transmitter, measures flows ranging from 0.001 kg/hr (0.00221 lbm/hr) to 1.5 kg/hr (3.3071 lbm/hr). Flow to the meters is

controlled by a dual line setup in combination with ¼ turn ball valves. Two different types of flow meter are used to accommodate all the flow rates required with highest accuracy possible.

3.1.3- Test Section Assembly

Test section assembly comprises of six parts. They are:

I) Tube insulation platform – It is constructed of 2 layer high duty foam tape with 1/8 inch in thickness. This kind of material is very easy to machine for making grooves necessary to fit the tubes, at the same time very effective on thermal insulation. Parker stainless steel reducing compression fittings of size 1.59 mm (1/16 inch) and 3.18mm (1/8 inch) are used to size down the test section assembly with the test section platform.

II) Polyimide ferrules – Tubes are tightened with the help of polyimide ferrules made of graphite supplied by Small Parts Inc. These ferrules act as a reducing fitting and bridge the gap between Parker stainless steel reducing compression fitting of size 1.59 mm (1/16 inch) and 3.18mm (1/8 inch) and the tubes.

III) Tubes – Tubes used for the experiment are Stainless Steel 316 tubes from Small Part Company, and Nickel tubes provided by VICI Valco Instruments. The Stainless Steel tubes are drawn from a die directly. The Nickel Tubes are made by a totally different method. The Nickel tubes are made by electroplating nickel over a diamond-drawn mandrel in a continuous process. This kind of manufacture process can make sure the inner face of Nickel tube is quite smooth. In this research four Stainless Steel tubes with different inner diameters have been tested. They are

1600μm, 1000μm, 762μm, and 560μm Stainless Steel tubes. Three different Nickel tubes were also used for the experiments. They are 1016μm, 762μm, and 508μm Nickel tubes. All the tubes have a length of 12 inch.

IV) Pressure Transducer – Validyne model DP15 pressure transducer (Figure 3.2) is used for collecting the required pressure drop measurements. Different diaphragms for different ranges of pressure can be tailored in the pressure transducer according to the need. For accurate data and covering the complete range from turbulent to laminar different diaphragms are very necessary. Diaphragms available in the research facility ranged from 0.08 to 200 psi (0.551-1397kPa). Validyne pressure transducer has an accuracy of ±0.25% using full scale of diaphragm. Pressure transducer was connected to the test section assembly by Parker stainless-steel compression tees and 1/4inch (0.635cm) OD PFA tubing. The signal from DP15 is transferred to the CD15 Sine Wave Carrier Demodulator (Figure 3.3). The CD15 Demodulator operates with variable reluctance transducers to provide a DC output signal for dynamics as well as steady state measurements. A 5kHz sine wave excitation is applied to the two inductance ratio arms of the transducer and the resulting output is demodulated and amplified using the latest integrated circuit techniques. The DC output is obtained from an active filter circuit and gives a uniform response from steady state to 1000 Hz. The low impedance sine wave excitation allows operation with the transducer located over 1,000 feet from the CD15. It outputs ±10 V DC which is directly proportional to pressure. Finally, its outputs will be connected to the NI Data Acquisition System.

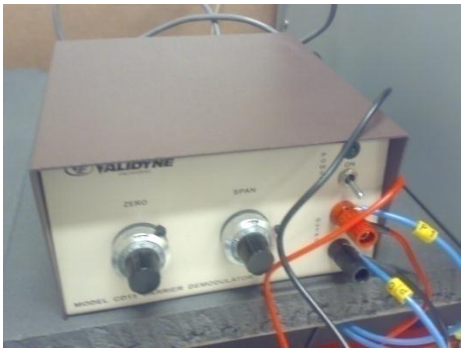

Figure3.2 Pressure transducer

Figure 3.3 CD15 Demodulator

V) Thermal probes – Two thermal probes of Omega model number TMQSS-020U-6 (Figure 3.4) are deployed in test section assembly at two locations one at the start of the test section and one at the end of it. By comparing the temperature difference of the inlet and outlet thermal probes we can calculate how much heat has been input into the water flow. Thermal probes are ungrounded with a length of 6 inch and a diameter of 0.508 mm (0.02 inch) and have an accuracy of ±0.5ºC (0.9ºF). Thermal probes are inserted in the flow by the use of two Parker stainless steel compression tees, while maintaining the required sealing.

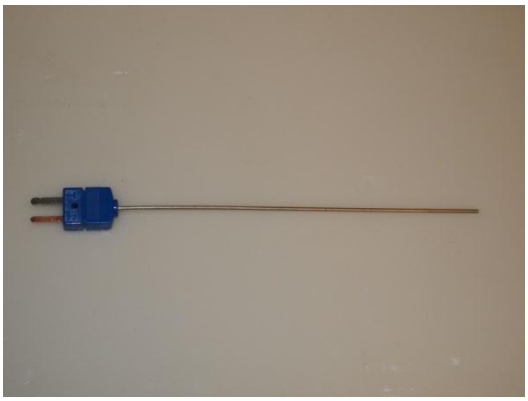

Figure 3.4 TMQAA-0.20U-6 Thermal probe

VI) Thermocouples – Thermocouples of Omega model number COCO-003 are used to test the surface temperature of testing tube. COCO-003 is a kind of type T thermocouple with 0.075mm (0.003 inch) diameter and 300 mm length. Due to the extremely small diameter, they are the ideal

instrument to be used to measure the temperature in a small surface like the micro-tube surface. At the same time they are very easily broken, so they need to be well protected before using. In this experiment vinyl tape is used to protect these small thermocouples. As Figure 3.5 shows the two legs of thermocouples were protected by two layers of vinyl tape. The Omega Bond was used to glue thermocouples to the tube surface. Omega Bond is a kind of glue with high thermal conductivity but electrically insulated. Omega Bond can protect the thermocouple from the DC current without effecting the temperature measurement.

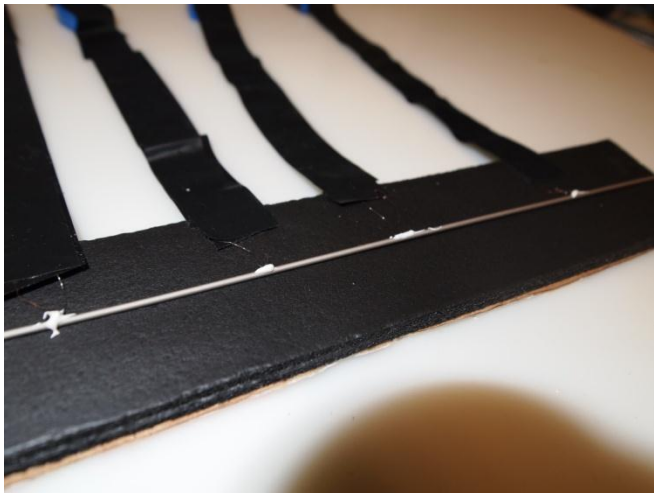

Figure 3.5 Thermocouples on the tube surface

3.1.4- DC Power Supply

The Power Supply input is 110V AC current and the maximum output of power supply is 60A DC. The DC output current can be adjusted from 0A to 60A continuously. The DC output lines were soldered on the two ends of testing tubes. At the same time, a voltage gauge has been used to measure the voltage of tubes' two ends. The input power can be calculate by the equation:

$$Q_{in} = I * V \qquad (1)$$

Where, Q_{in} = Input power by power supply, I =Input DC current, and V=Input voltage.

3.1.5- Data Acquisition System

The data collected by the pressure transducer and thermocouples were sent to National Instruments data acquisition system and recorded by a LabView program. Data acquisition system has three major parts in its structure:

- Chassis –The chassis is the rack mounted with SCXI 1001. Chassis basic function is to provide a shielded enclosure with forced air cooling and USB connection to the laboratory PC.
- Input Module – module used is SCXI 1102, which is connected directly with the chassis and performs the operation of signal conditioning and functions as a port of connection for the terminal blocks. The above mentioned module has thermocouple input with 32 input channels, receives the signal input from thermocouple. Maximum sampling rate for the received input is 333,000 samples per second.
- Terminal Block – As mentioned earlier input module acts as port of connection for terminal blocks, so terminal block act as an input module for thermocouples. Terminal block used is SCXI 1303. It is a 32 channel terminal block isothermal construction minimizing the error due to temperature differences between the terminals and the cold junction sensor, giving high accuracy thermocouple measurements. Also this terminal block provides automatic ground referencing for the ungrounded thermocouples used in the set up.

3.2 Calibration

For any experimental setup to give accurate measurement calibrating the instruments is the most important task. Experimental setup used in this research has three very important components, which require checking for calibration, they are Omega thermocouples/ probes, Micro Motion Coriolis flow meter and Validyne pressure transducer.

3.2.1-Pressure Diaphragms Calibration

Validyne pressure transducer needs special attention with reference to calibration because diaphragms are changed frequently requiring the transducer to be re-calibrated. It also becomes important because erroneous reading with pressure drop will lead to bad friction factor calculations.

Six pressure diaphragms ranging from 8-200 psi were used for capturing the complete range of pressure drops. These diaphragms were calibrated by comparing the voltage output of the differential pressure transducer when applied different pressure with four research grade test gauges. Calibration is performed every time before starting the experiment and when the diaphragm is changed.

Illustrated below are the stepwise procedures for calibrating the Validyne pressure transducer.

- Appropriate diaphragm is chosen according to the need of the experiment, starting with the largest range.
- Place the diaphragm inside the Validyne pressure transducer and check for the two O-rings, that they are not displaced from their position.
- Tighten up all the screws so that there is no leakage when pressurized.
- Connect the positive port of the transducer to the calibration pump.
- Connect the other end of calibration pump to the research grade test gauge.

- Make sure pressure transducer is connected to carrier demodulator and is turned on, carrier modulator's job is to pass the signals to the data acquisition system where the job of evaluation between voltages to the pressure applied is done.
- Tighten all the nuts connecting the pressure transducer to the pump, and check for any leakage.
- Bleed all the entrapped air in the pump, and check for the reading of the gauge to be zero before the pumping is turned on.
- Open up the module on laboratory computer stating as DPS -15 calibration
- Save the module file at appropriate location.
- Assign a name to the file, and now we are ready to record the data.
- Adjust span in the carrier demodulator, such that at maximum pressure of the diaphragm, maximum voltage achieved is 10 Volt or less than that. Maximum voltage should not exceed 10 Volt.
- Record the first point at zero psi for calibration.
- After recording zero psi, make 5 the same size increments for the diaphragm, pump the air and record at each and every increment.
- Now when recording for each and every increment observe the pressure gauge needle that it is at the exact point where it's supposed to be, if required make fine adjustment by the adjustment knob on the pump.
- After following the above mentioned for each and every increment, record the voltage at that increment.
- Once all the points are recorded, a graph is plotted between voltage versus pressure.
- From the graph obtain the trend line equation for the graph which is the calibration equation desired, check for the correlation coefficient R^2 value that it is either 1 or close to 1. R^2 is one way of ascertaining that the calibration equation obtained is accurate. If R^2 value is less than 0.99 redo the calibration.

This completes calibration of Validyne pressure transducer. Figures 3.6 shows an example plot of pressure versus voltage for 125 psi diaphragm along with its calibration equation and R^2 value. Calibration of 125 psi diaphragm has a total of 6 points with an increment of 25 psi. In this plot we can obtain the calibration result: y=13.205x+0.2573, where y= pressure (psi), and x= voltage (V). Opening the obtained file from LabView in Microsoft excel and adding the trend line to the points gives the calibration equation. This calibration equation obtained is substituted in the LabView module which records the data from pressure transducer and thermocouple and it governs how pressure transducer is going to perform.

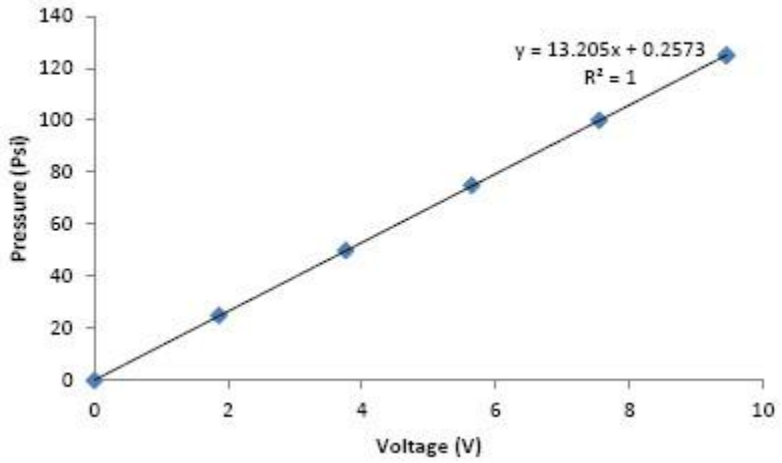

Figure 3.6 Calibration curve for 125 psi diaphragm

3.2.2-Thermocouple Calibration

The accuracy of the thermocouples directly affects the final result. The thermocouples should be carefully installed and calibrated. Some of the researchers use the pre-calibrated thermocouples without verification. The manufacturer usually calibrates the thermocouple by selecting a few points in a large temperature range, but most of the heat transfer experiments are done at a

relatively narrow range of $20\,°C$ to $40\,°C$. In order to get the most accurate results, it's necessary to calibrate the thermocouples in the specific temperature range. When the thermocouples are attached to the tube's surface they are usually surrounded by some type of glue. This is another factor that may affect the thermocouples measurement, as the glue may cause a temperature difference between the thermocouple and the tube. It's necessary to develop a customized calibration procedure to calibrate the thermocouples that are used to measure the surface temperature of a micro-tube. In this experiment all the thermocouples were calibrated by a temperature bath. The temperature bath can provide a constant temperature by heating or cooling the water. The thermocouples can be calibrated by comparing with the water temperature and the temperature read from the thermocouple.

Procedures for calibrating the thermocouples:

1. Attach thermocouples to the tube that is to be tested.
2. Fill the temperature bath with pure water.
3. Submerge the tube and thermocouples into the water.
4. Decide on the temperature range that thermocouples are to be used.
5. Set the temperature bath to the lowest temperature in the range.
6. Waite for the water temperature in the bath to become stable.
7. Record the temperature that you set for the bath and the temperature that you read from thermocouples.
8. Increase the temperature of temperature bath by 1°C and repeat step 7. After you have reached the highest temperature in your range, shut down the temperature bath and take out the tube and thermocouple from the temperature bath.
9. Build a linear correlation of the temperature setting of the temperature bath and the temperature read from the thermocouples.

Figure 3.7 shows one of the thermocouple's calibration results. From the figure it can be seen that there is little difference between the actual temperature and the temperature measured by the thermocouple. The difference can be corrected by the calibration result:

$$y = 1.010 * x - 0.502$$

Where x= temperature measured by thermocouple, and y= actual temperature

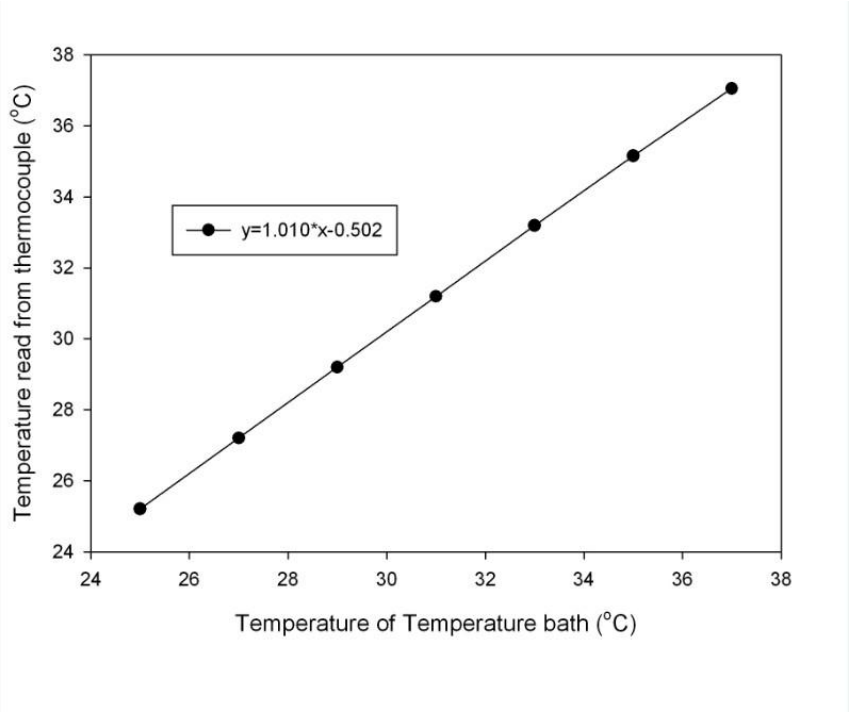

Figure 3.7 The calibration result of a thermocouple

3.2.3- Flow Meter Calibration

Micro Motion Coriolis flow meter was factory calibrated. For CMF -025 manufacturer's specified tolerance for calibration error is ±0.1%. For LMF3M, manufacturer's calibration tolerance is ±1.0%. Also in addition the maximum and minimum milliamp outputs of the CMF-025 were fine-tuned to make sure the output single in an appropriate range.

3.3 Experimental Procedure

3.3.1- Heat Transfer

1) Attach thermocouples on the tube that is to be tested.
2) Calibrate the thermocouples.
3) Connect the testing tube to the fluid delivery system.
4) Connect the DC power to the tube.
5) Use foam tape to insulate the tube.
6) Turn on the data acquisition system.
7) Open the nitrogen tank and increase the pressure in the water tank.
8) Fully open the water tank valve and let the water flow go through the system.
9) Check the leakage and data acquisition system.
10) Adjust the metering valve to the Renolyds number that is to be tested.
11) Turn on the DC power supply and adjust the current.
12) Wait for a while until the tube reaches steady state.
13) Take the data for 30 seconds and then stop the data acquisition system.
14) Turn off the DC power supply.
15) Close the water tank valve.
16) Perform data reduction.

3.3.2-Pressure Drop under Different Heat Transfer Rate

1) Connect the Validyne pressure transducer with the appropriate calibrated diaphragm affixed in it, start with the largest range diaphragm.
2) Open the nitrogen tank valve, and make sure the pressure is under the water tank's pressure limit.

3) Open the water tank valve and the water will flow through the system. Check every possible leakage on the system.
4) Make sure the bubbles inside the pipeline have been bled out.
5) Turn on the flow meter and data log system.
6) Adjust the metering valve to fix the water flow to a certain Reynolds number.
7) Wait for a few minutes until the reading of pressure drop is stable.
8) Log the pressure drop data for one minute. Then stop data logging.
9) Turn on the DC power supply and adjust the current until the inlet and outlet water temperature difference is about 3°C.
10) Waite for about 20 minutes until the testing tube reaches a steady stable status. You may need to adjust the DC current again during this process to make sure the inlet and outlet temperature difference is about 3°C.
11) Repeat steps 8 to 10, but this time the temperature difference of inlet and outlet will be set as 5°C.
12) Turn off the DC power supply and close the water tank output valve.
13) Close the nitrogen tank outlet valve and release the pressure in the water tank.
14) Refill the water tank and start the next Reynolds number. Repeat step 1 to step 13, but change the diaphragm if necessary.

3.4 Testing Tubes Measurement

The previous master students Wendell L. Cook (Cook, 2008) has done the inner surface roughness and diameter measurements for stainless steel tubes and Atul Singh (Singh, 2011) has performed the Nickel tubes inner surface roughness and diameter measurements. Their measurement results were used in this experiment. 4 Stainless Steel tubes and 3 Nickel tubes have

been tested in this experiment. There are two parameters that need to be measured or verified. They are 1) Diameter, 2) Roughness.

The inside diameter has been given by the manufacturer companies already. In this experiment the inside diameter has been verified by using a Scanning Electron Microscope (SEM) at Oklahoma State University microscopy lab. Two stainless steel tubes were examined. The first of these two tubes had an inner diameter and tolerance of $5330 \pm 76 \mu m$. The second tube examined had an inner diameter and tolerance of $584 \pm 38 \mu m$. Nickel tube that was selected for this examination was with the diameter and tolerance of $762 \pm 25 \mu m$. Thus, a broad range of tube sizes was covered between these tubes examined. Imaging was done using JEOL JXM 6400 Scanning Electron Microscope System in combination with a digital camera, resolution of the microscope ranged from 30-50 nm. After capturing the image based on the scale of the picture, the inner diameter of the tube was estimated by measuring the image pixels. For the first stainless steel tube with manufacturer-specified inner diameter of $5330 \pm 76 \mu m$ the average inner diameter was estimated to be 5280 μm from the SEM image. For the second stainless steel tube with the manufacturer-specified inner diameter of $584 \pm 38 \mu m$, the average inner diameter was estimated to be 574 μm from the SEM image (see Figure 3.8). The selected $762 \pm 25 \mu m$ Nickel tube's diameter was found to be 782µm (see Figure 3.9), so that the estimated Nickel tube diameter was within ±2.62 % of the specified diameter, which was within ±3.33 % of the manufacturer's specification.

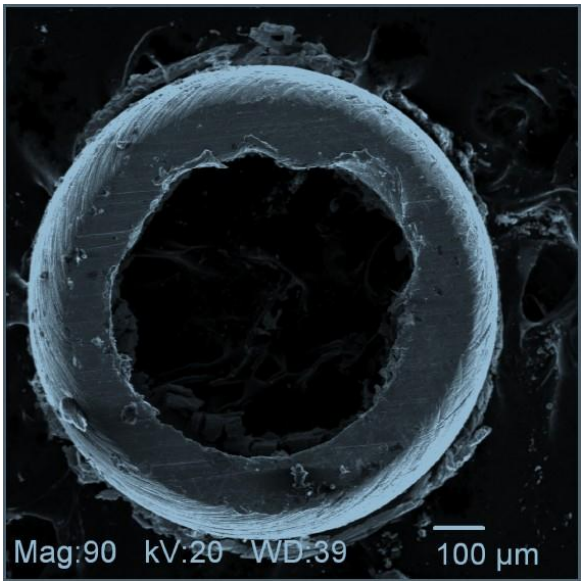

Figure 3.8 SEM image of a 584±38µm (manufacturer's specification) diameter stainless steel tube; based on this SEM image, the tube diameter was found to be 574µm.

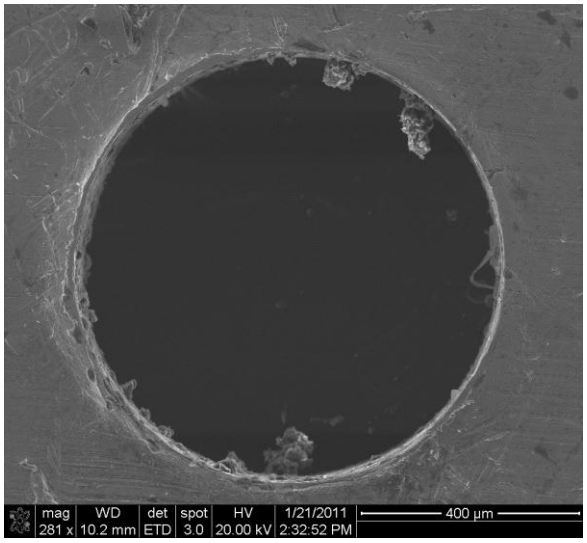

Figure 3.9 SEM image of 762±25 µm (manufacturer's specification) diameter Nickel tube. Based on this SEM image tube diameter was found to be 782 µm.

Roughness of stainless steel tube measurements were conducted using a SPM station in combination with Digital Instruments Multimode V electronics and an optical microscope for tip positioning. The system used is capable of three-dimensional (3-D) spatial mapping with an

ultimate resolution of 0.1 nm laterally and 0.01 nm vertically. Scans were taken of multiple sections of two stainless steel tubes with different inner diameters: 5,330μm and 2,390μm. Roughness data were taken from three different sections of each of these tubes. In order to negate the effect of the curvature of the tubes upon the roughness measurement generated by the SPM, a flattening feature was utilized. From the SPM, information such as average roughness (R_a), maximum roughness profile peak height (R_{max}), and root mean square roughness (R_q) of the samples was obtained. The topographic image for a section of the 5,330μm diameter tube is shown in Figure 3.10.From the SPM measurements, the inner surface of the 5,330μm diameter stainless-steel tube has average roughness (R_a),maximum roughness profile peak height (R_{max}), and root mean square roughness (R_q) of 240 nm, 2,628 nm, and 292 nm, respectively. In similar manner, the inner surface of the 2,390μmdiameter stainless-steel tube has Ra, R_{max}, and R_q of 150 nm, 1710 nm, and 194 nm, respectively. Some variability was found between the two tubes, though this was to be expected. The manufacturer specified an inner wall root mean square roughness of 410 nm. Thus, the root mean square roughness measured by the SPM for each of the two tubes was within the manufacturer's specifications.

When compared with the roughness results documented by Young et al. (2009), the maximum roughness profile peak height (R_{max}) for both stainless-steel tubes falls between the maximum roughness profile peak height of milled stainless-steel surface (R_{max} = 3210 nm) and ground stainless-steel surface (R_{max} =999 nm). It should be noted that measurements by Young et al.(2009) were from surface roughness that was created systematically to be uniform and aligned. On the other hand, the tubes used in this study were obtained commercially and thus the uniformity and alignment of the surface roughness in these tubes are uncertain.

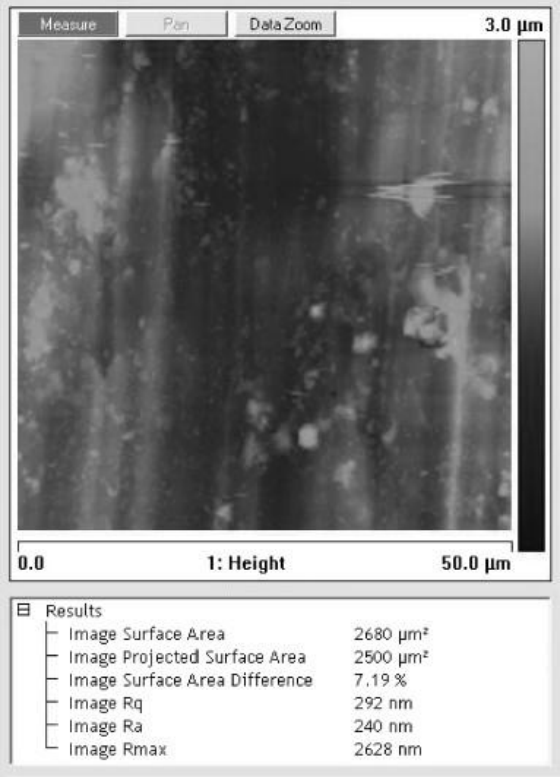

Figure 3.10 SPM topographic image for a section of a 5,330µm inner diameter stainless steel tube (R_a = 240nm, R_{max} = 2,628nm, R_q = 292nm).

The Nickel tubes are made by electroplating nickel over a diamond-drawn mandrel in a continuous process. When the mandrel is removed from the tubing, an internal surface with a mirror-like 1-2 micro inch finish remains on. So the roughness of Nickel tubes is relatively small. According to the previous measurements the roughness of the Nickel tubes inner surface is about 51nm.

After all the tubes' parameters have been measured or verified the testing tubes' specifications have been tabulated in Table 8.

Table 8 Approximate Diameter Roughness and Relative Roughness of Testing Tubes

stainless steel		
Inner Diameter(D)	**Root Mean Square Roughness(ε)**	**Relative Roughness (ε / D)**
1600 μm	16.51 μm	1.03%
1000 μm	16.51 μm	1.65%
762 μm	16.51 μm	2.17%
560 μm	16.51 μm	2.94%
Nickel		
1016 μm	51 nm	0.005%
762 μm	51 nm	0.006%
508 μm	51 nm	0.01%

3.5 Constricted Flow Parameters

In all the studies performed on micro-tubes for friction factor calculation tube inner diameter was taken directly into calculations. Recently Kandlikar et al. (2005) proposed a new way of looking at the diameter based on constricted flow parameters. This part of chapter reviews the constricted parameters and the new equation proposed for calculation of friction factor, explaining constricted parameters and how the new friction factor equation evolves out of it. Equation is later used on different data sets.

Starting with defining constricted parameters, a micro-tube has a diameter D but with roughness all around the inner walls of tube, parameter $D_{h,cf}$ represents new constricted diameter. ε_{FP} is

roughness element height based on the proposed constricted parameters. The parameters can be understood better by referring to Figure 3.11.

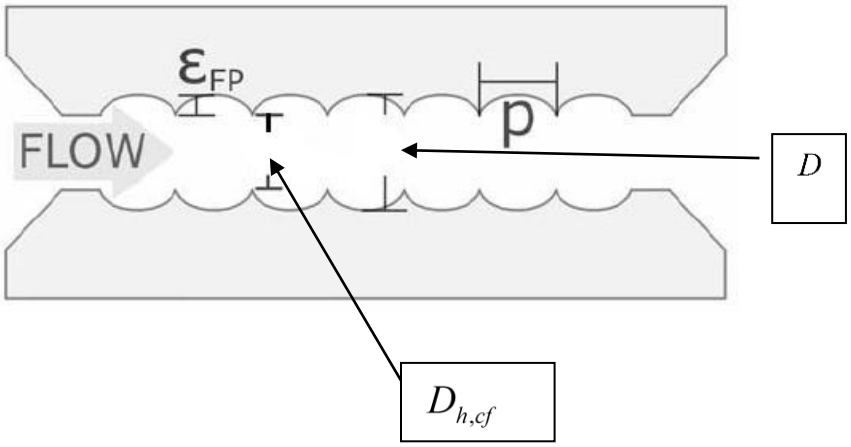

Figure 3.11 Side view of micro-tube with parameters marked [Kandlikar et al.(2005)].

The curved surface represents the roughness profile. It is assumed to be even throughout the tube even though it might not be the case in practice. It should be noted that pitch p of roughness element does not play any role in the uniform roughness assumed for the development of constricted flow equations.

To calculate the new constricted parameters, $D_{h,cf}$, A_{cf} and P_{cf} are defined as follows

$$D_{h,cf} = D - 2\varepsilon_{fP} \qquad (2)$$

$$A_{cf} = \frac{\pi D_{cf}^2}{4} \qquad (3)$$

$$P_{cf} = \pi D_{cf} \qquad (4)$$

Based on the parameters defined above, equation for the constricted flow friction factor proposed by Kandlikar et al. (2005) is given by Eq. (5).

$$f_{cf} = \frac{fD_{cf} A_{cf}^2}{DA^2} \qquad (5)$$

Constricted Reynolds number is calculated by using Eq. (6)

$$\mathrm{Re}_{cf} = \frac{4\dot{m}}{\mu P_{cf}} \qquad (6)$$

A major purpose of using the constricted parameters proposed by Kandlikar et al. (2005) is that it effectively predicts the friction factor for laminar region. This method steers back the friction factor value for laminar region back to theoretical laminar line therefore, reducing the roughness effect in laminar region. Using the friction factor and Reynolds number Equations (5) and (6), Brackbill & Kandlikar (2007) proposed two correlations. It was recommended that use of these correlations provide a method for prediction of the critical constricted Reynolds number, for not so smooth tubes to the point of smooth channels of similar geometric parameters.

3.6 Experimental Uncertainties

3.6.1- Friction Factor

To understand the uncertainties in the friction factor data presented, the Darcy equation (Eq.7) has been used to calculate the experimental friction factor values.

$$f = \frac{2\Delta PD}{\rho LV^2} \qquad (7)$$

Looking at velocity term in (Eq.7) velocity is calculated from mass flow rate equation which contains area term in it (Eq.8) which is rearranged as shown in (Eq.9)

$$\dot{m} = \rho A V \qquad (8)$$

$$V = \frac{\dot{m}}{\rho A} \qquad (9)$$

The area is given by (Eq.10)

$$A = \frac{\pi D^2}{4} \qquad (10)$$

Therefore

$$V = \frac{2\Delta P D^5 \rho \pi^2}{16 L \dot{m}^2} \qquad (11)$$

Substituting this value of 'V' in (Eq.11) we get equation for friction factor as (Eq.12)

$$f = \frac{2\Delta P D^5 \rho \pi^2}{16 L \dot{m}^2} \qquad (12)$$

From the above equation (Eq.12) it is observed that there are five different variables upon which the uncertainty in calculation of friction factor depends. These are (1) Pressure drop, (2) Tube inner diameter, (3) Density, (4) Tube length and (5) Mass flow rate. Looking at uncertainties by each factor discretely it should be noted that pressure drop, tube length and mass flow rate can be controlled in the laboratory. Tube inner diameter uncertainty depends upon the manufacturers specifications and manufacturing accuracy, tube inner diameter does not represent the accuracy of experimental setup. However Scanning Electron Microscopy is used to ensure and measure tube inner diameter.

First looking at pressure drop uncertainty, pressure drop is obtained by using Validyne pressure transducer and as mentioned earlier specification of the transducer is ±0.25 % of the full scale reading of each diaphragm used. To further reduce the uncertainty, diaphragms were carefully selected in order to obtain the highest accuracy possible and covering the maximum range. To confirm the accuracy of the diaphragm, over lapping the lower end of one diaphragm with upper end of the next diaphragm was made mandatory. Even though after taking such attention worst situation occurs with small tubes and low Reynolds number, and estimation of uncertainty in this situation is important. For this situation uncertainty in the pressure drop measurement was found to be ±1% of reading. Looking at the intermediate sized tubes and flow rates, uncertainty in pressure drop measurement is ±0.4% of reading when pressure transducer is pushed to its limits.

Mass flow rate is measured by Micro Motion flow meter and specification for high flow meter CMF-025 meter is ±0.5% of reading and it is used for high flows and larger tubes, but it should be noted that this flow meter is used for flow ranges lower than its range to cover the entire range of flow rates for the tube under experiment. Low flow meter LMF3M meter specification is ±0.5%. Based upon the uncertainty equation provided by the flow meter manufacturer the maximum uncertainty between two meters is ±1.8%. Thus the above mentioned data helps in determining the uncertainty in mass flow rate.

Tube length uncertainty is determined by the accuracy in cutting the high density polyethylene tube cradles, in which the tube is mounted for experiment. Length of the cradle serves as a reference for mounting the tube sections ensuring consistency in the tube length. Measured uncertainty in the cradle lengths is ±0.26% of length.

The water density used is 0.9972995g/cm^3 which is measured under 24 °C. The highest water's temperature in this experiment is 26°C and the lowest is 22°C. The density of water is 0.9967867 g/cm^3 and 0.9977735 g/cm^3, respectively. So the overall uncertainty of water density is ± 0.05%.

Four different uncertainty values have been established till now. In order to estimate overall uncertainty, an analysis was conducted using the Kline and McClintock (1953) method for estimation of overall uncertainty. For larger tube sizes and high Reynolds numbers, the CMF-025 meter is used and is functioning at the manufacturers' specified uncertainty level. The pressure transducer is operating at the better of its two calculated uncertainty levels. Taking this into consideration, the overall uncertainty is calculated at ±0.83%. For small tube size and low Reynolds number, the CMF-025 meter begins to operate under range. In this area, the pressure transducer is considered to be operating at the lesser of its two uncertainty levels. In this range, the overall uncertainty associated with the experimental apparatus is calculated at ±2.78%. Finally, for the lowest ranges of tube size and Reynolds number, the LMF3M meter is used, the pressure transducer is still operating at the lesser of its two uncertainty levels. For this lowest Reynolds number and smallest tube size situation, the overall uncertainty decreases to ±1.51%. The final uncertainties for these 5 variables and friction factor have been listed in Table 9.

Table 9 Uncertainties of Friction Factor Measurement

	Pressure Drop	Tube inner diameter	Density	Tube length	Mass flow rate	Friction factor
Uncertainty	±1%	±1.7%	± 0.05%	±0.26%	±1.8%	±0.83% to ±2.78%

3.6.2- Heat Transfer

For heat transfer the flowing equation is used to calculate the heat transfer coefficient.

$$h_i = \dot{q}_i^{''} / (T_{wi} - T_b) \quad (13)$$

Where h_i =local heat transfer coefficient, $\dot{q}_i^{"}$ =local inside wall heat flux, T_{wi} =local inside wall temperature at the thermocouple location and can be calculate by finite-difference formulations proposed by Ghajar and Kim (2006), and T_b =bulk fluid temperature at the thermocouple station.

In this equation $\dot{q}_i^{"}$ can be calculated by the following equation.

$$\dot{q}_i^{"} = \frac{\dot{Q}_i}{A_i} \qquad (14)$$

Where $\dot{Q}_i$ =inside heat transfer rate, and A_i =tube inner surface area.

The inside heat transfer rate can be calculated by the following equation.

$$\dot{Q}_i = \dot{m} c_p (T_e - T_i) \qquad (15)$$

Where $\dot{m}$ = mass flow rate, c_p =specific heat of water at constant pressure, T_e = outlet water temperature, and T_i = inlet water temperature.

In this experiment the tubes are under constant wall heat flux condition, the bulk fluid temperature increases linearly from the inlet to the outlet according to the following equation:

$$T_b = T_{in} + (T_{out} - T_{in}) x / L \qquad (16)$$

Where x= the local length from water inlet.

The heat transfer coefficient can be expressed by:

$$h_i = \{[\dot{m} c_p (T_e - T_i)] / A_i\} / \{T_{wi} - [T_{in} + (T_{out} - T_{in}) x / L]\} \qquad (17)$$

And the Nusselt number can be calculated by

$$Nu = \frac{h_i D_i}{k} \tag{18}$$

Where D_i = inner diameter, and k = thermal conductivity of water.

Finally the Nusselt number can be written as

$$Nu = \frac{\{[\dot{m}C_p(T_e - T_i)]/A_i\}/\{T_{wi} - [T_{in} + (T_{out} - T_{in})x/L]\}}{k} * D_i \tag{19}$$

From the above equation we can see that there are 4 measured parameters that affect the uncertainty of the final heat transfer results. They are mass flow rate, temperature, length, and tube diameter. As the uncertainty of length, mass flow rate and tube diameter have already been discussed in friction factor uncertainty analysis, the only parameter that need to be investigated in the section was temperature measurement.

The outer surface temperature was measured by type-T thermocouples that were purchased from Omega Inc. The reported accuracy of these thermocouples by the manufacturer was ±0.1°C. In this experiment the thermocouples working temperature ranged from 25°C to 35°C, so the temperature measurement uncertainty is within ±0.4%.

The non-measured parameters for equation (19) were thermal conductivity and specific heat of water. In this experiment the thermal conductivity of water and specific heat of water were calculated by equations (20) and (21) that proposed by Ghajar and Kim (2006).

$$\begin{aligned} c_P = {} & 4219.8728 - 3.3863T + 0.11411T^2 - 2.1013\times10^{-3}T^3 + 2.3529\times10^{-5}T^4 \\ & - 1.4167\times10^{-7}T^5 + 3.58520\times10^{-10}T^5 \end{aligned} \tag{20}$$

Where c_P = specific heat, J/(kg-k) and T=temperature, °C

$$k = 5.6026\times10^{-1} - 2.1056\times10^{-3}T - 8.6806\times10^{-6}T^2 - 5.4451\times10^{-9}T^3 \tag{21}$$

Where k = thermal conductivity of water, W/(m-K) and T = temperature, °C

From equations (20) and (21) we can calculate that the uncertainty of specific heat and thermal conductivity of water was less than 0.1%, when the temperature measurement accuracy was ±0.1°C.

Until now all 6 parameters' uncertainties have been established. In order to estimate overall uncertainty of Nusselt number, an analysis was conducted using the Kline and McClintock (1953) method for estimation of overall uncertainty. The result showed that the uncertainty for Nusselt number in this experiment was calculated at ±15.6%. Table 10 listed all the uncertainty values for these measured parameters and Nusselt number in this heat transfer experiment.

Table 10 Uncertainties of Heat Transfer Measurement

	Tube inner diameter	Tube length	Mass flow rate	Temperature measurement	Nusselt number
Uncertainty	±1.7%	±0.26%	±1.8%	±0.4%	±15.6%

CHAPTER IV

RESULT AND DISSCUSSION

4.1 Friction Factor Results

Before discussing the friction factor results in micro tubes, it is necessary to revisit some of the results that have been found by previous researchers. As Table 2 showed, the results are not consistent with each other. However, it is not hard to see that there exist only two different kinds of results: higher than conventional theory and agree with conventional theory. Few of them find the friction factor value is lower than conventional theory. The conventional theory here refers to the friction factor equation given by Poiseuille for fully laminar region f=64/Re and Blasius friction factor equation for turbulent flow $f=0.316/Re^{0.25}$. Table 1 shows that the testing tube's material can be divided into two parts also: stainless steel and non stainless steel material. Focusing on the stainless steel tube's results, most of researchers found that the friction factor value for relatively small diameter (less than 600μm) stainless steel tubes is higher than the conventional theory. Considering these tubes' large inner surface roughness and small diameter, all these tubes have a large relative roughness. The higher friction factor value may be caused by the large relative roughness value. In order to verify this four stainless steel tubes have been tested in the current research work.

In the current experimental work, the friction factor has been measured under isothermal and constant heat flux conditions for four stainless steel tubes. These tubes have different diameter

size but have the same inner surface roughness (410nm). The smallest 560μm tube has the largest relative roughness (0.068%). The isothermal run results have been plotted in Figure 4.1.

Figure 4.1 shows that reducing the tube diameter from 1600 μm to 762μm did not significantly affect the profile of the friction factor and the friction factor value agrees well with conventional theory. However, as the tube diameter is further decreased, the friction factor profile shifted upward. From Figure 4.1 we can see that the 560μm tube data has been separated from the larger size tubes group (1600μm, 1000μm, and 762μm) in all the flow regions. The friction factor value for 560μm is 30% higher than conventional value in laminar region and 15% higher in turbulent region. This can be explained by the largest relative roughness value of 560μm tube among these four tubes. The large relative roughness is the reason why small diameter stainless steel tubes have higher friction factor value.

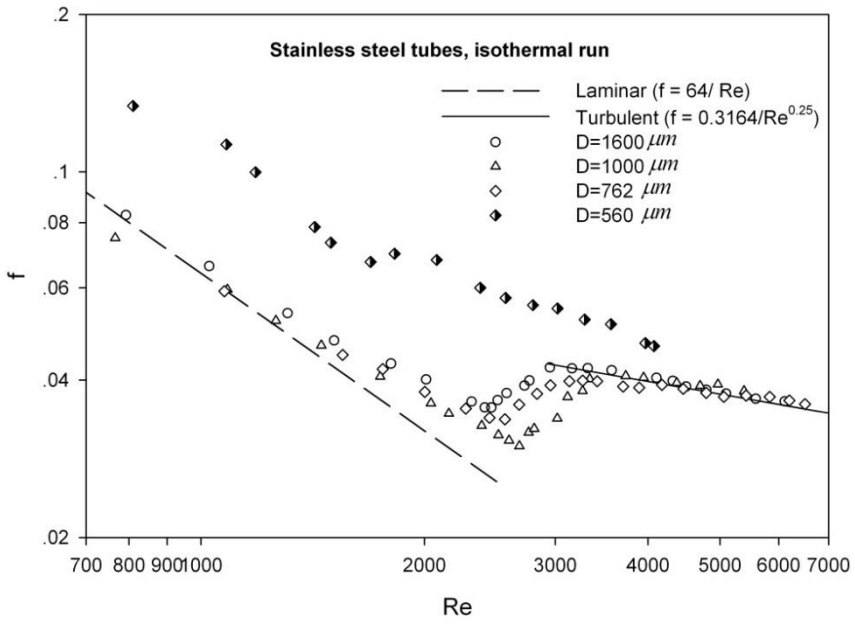

Figure 4.1 Friction factors of stainless steel tubes from 1600μm to 560μm under isothermal condition.

Before this experiment, Ghajar et al. (2010) have already done some research work about friction factor of stainless steel tubes in the transition region. Their results will be reviewed before discussing the current friction factor results. Figure 4.2 and Figure 4.3 show the results from Ghajar et al. (2010). In their results, the start and end of transition changed when the tube diameter changed. For pipe diameters ranging from1372 to 838μm the start of transition shifted to higher Reynolds numbers (see Figure 4.2). For pipe diameters ranging from 838 to 337μm the start of transition shifted to the lower Reynolds numbers (see Figure 4.3).

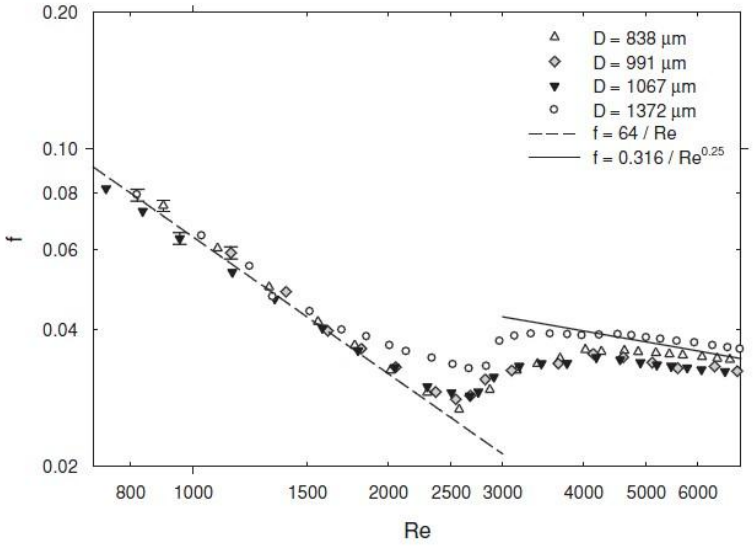

Figure 4.2 Transition region of stainless steel tubes with diameter from 1,372 to 838μm. [Ghajar et al. (2010)].

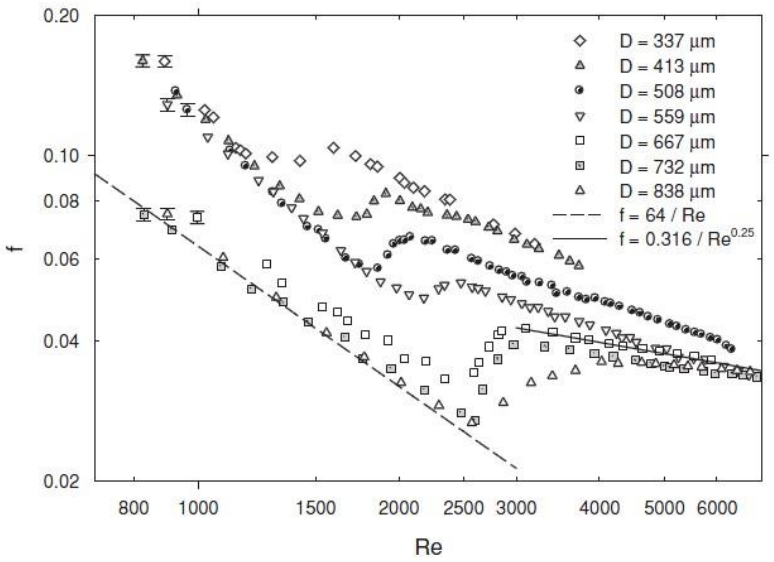

Figure 4.3 Transition region of stainless steel tubes with diameter from 838 to 337µm. [Ghajar et al. (2010)].

Going back to the current experimental results and focusing on the transition region, isothermal run results that depicted in Figure 4.1 show that when the diameter decreased from 1600 μm to 1000 μm the transition region shifted to the higher Reynolds numbers. It means that both the start Reynolds number and the end Reynolds number for transition region increased. As Table 11 shows the start Reynolds number for transition region is 2442 for 1600µm tube and increases to 2670 for 1000µm tube. The end Reynolds number is 2949 for 1600µm tube and increases to 3725 for 1000µm tube. But when the tube diameter continually reduced from 1000 μm to 560 μm , the transition region shifted to the opposite direction. The transition region start Reynolds number for 762µm tube is 2265 which reduced by about 400 compared with the 1000µm tube. For the 560µm tube it shifts to even smaller Reynolds number of 1675. The transition region end Reynolds number for 762µm and 560µm diameter tubes are 3129 and 2082, respectively. This kind of transition region shift is caused by the relative roughness difference in these tubes.

Table 11 The Start and End Reynolds Number of Transition Region for 4 Stainless Steel Tubes and 3 Nickel Tubes.

	Isothermal Friction Factor		$\Delta T = 3°C$ **Heating Friction Factor**		$\Delta T = 5°C$ **Heating Friction Factor**		**Heat Transfer** $\Delta T = 3°C$	
stainless steel	Re_{start}	Re_{end}	Re_{start}	Re_{end}	Re_{start}	Re_{end}	Re_{start}	Re_{end}
1600 μm	2442	2949	2455	3076	2492	3158	2504	3097
1000 μm	2670	3725	2756	3807	2848	3972	2593	3147
762 μm	2265	3129	2327	3302	2378	3466	2306	3128
560 μm	1675	2082	1730	2155	1807	2203	2443	3039
Nickel								
1016 μm	2219	3386					3207	3954
762 μm	2823	4062					3734	4860
508 μm	2337	3076					3363	4109

For friction factor under constant heat flux condition, as Figure 4.4 to Figure 4.8 show, the friction factor value decreased in comparison to the friction factor under isothermal condition in laminar and transition regions. The reduction of friction factor under heating condition is due to the decrease in the viscosity as the temperature near the tube wall is increased. But for the end of the transition region and turbulent region the heating effect on friction factor became weaker. For transition region, the start Reynolds number is delayed by heating. For example, the transition start Reynolds number is 2442 for 1600μm tube under isothermal run, and this number is delayed to 2455 when the inlet and outlet temperature difference is 3ºC (see Figure 4.4). For the inlet and outlet temperature difference of 5ºC, the transition start Reynolds number is further delayed to

2492 as shown in Figure 4.4. Similar trends are observed in Figures 4.5 to 4.7 for the tube diameters of 1000μm, 762μm and 560μm, respectively. Tam et al. (2011) is the only publication that discussed the heating effect on friction factor in micro tubes and their results have been show in Figure 4.8. From Figure 4.8 their experimental results are similar to the current results, but their results are agreed well with the conventional theory in the laminar and turbulent regions. That is due to the relatively larger tube diameter (≥700μm) used.

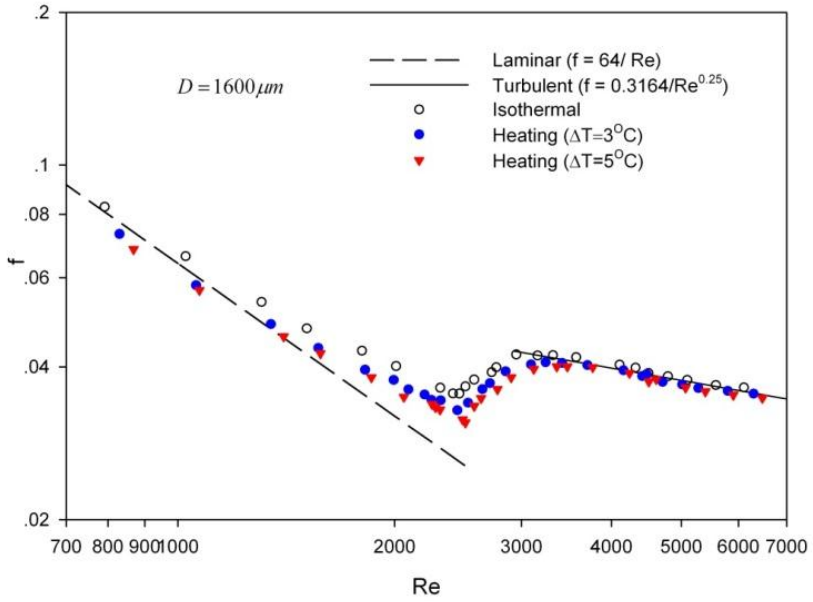

Figure 4.4 Friction factor of 1600μm stainless steel tube under heating and isothermal conditions.

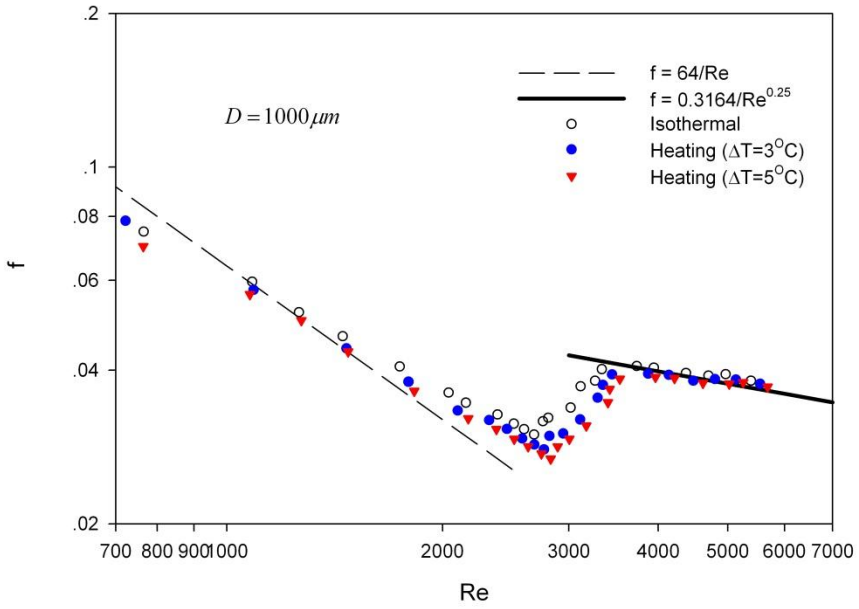

Figure 4.5 Friction factor of 1000μm stainless steel tube under heating and isothermal conditions

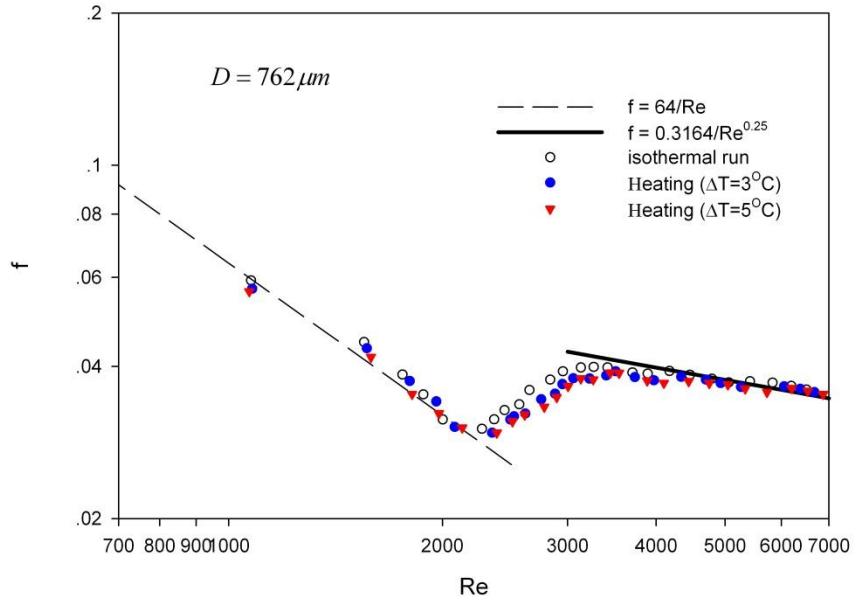

Figure 4.6 Friction factor of 762μm stainless steel tube under heating and isothermal conditions

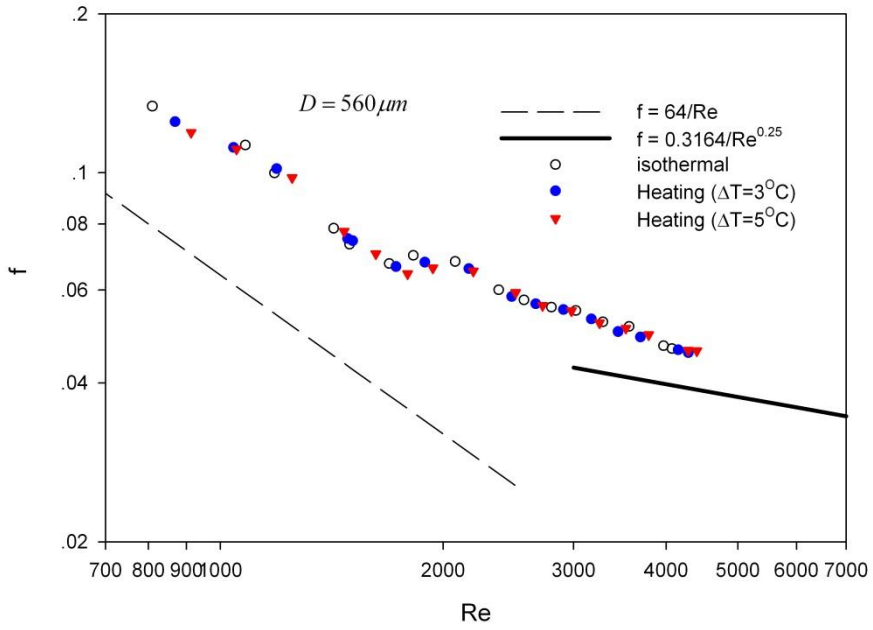

Figure 4.7 Friction factor of 560μm stainless steel tube under heating and isothermal conditions

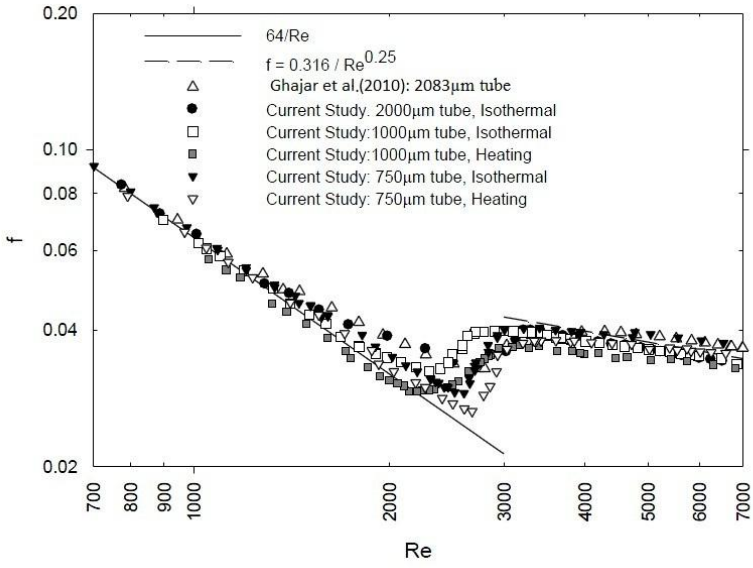

Figure 4.8 Friction factor characteristics for the macro- and micro-tubes under isothermal and heating boundary conditions. [Tam et al. (2011)].

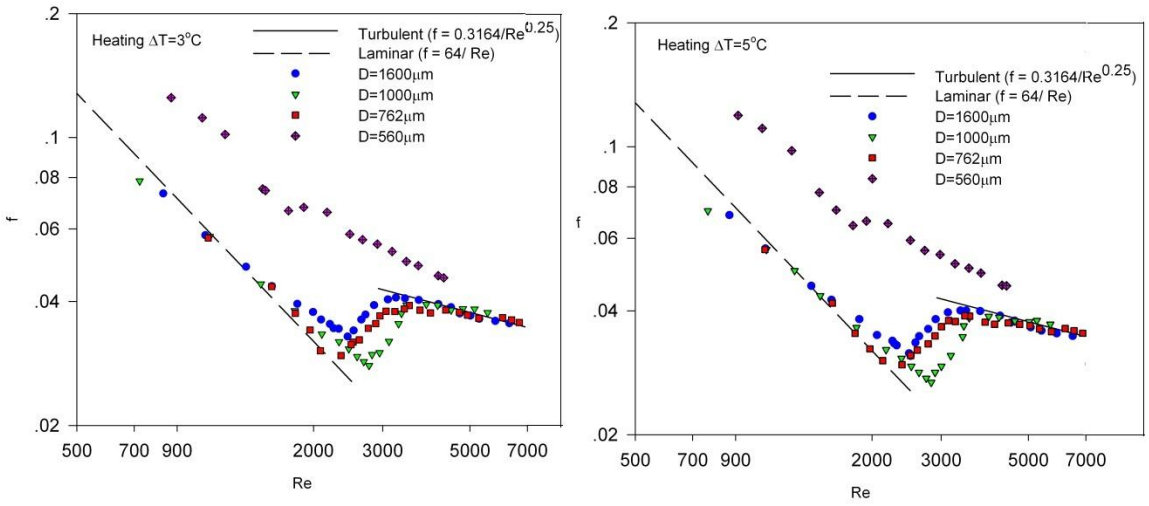

Figure 4.9 Friction factor of stainless steel tubes under heating condition (ΔT=3°C and ΔT=5°C)

Figure 4.9 shows the friction factor result for the four tested stainless steel tubes under the heating conditions (ΔT=3°C and ΔT=5°C). Comparing with the isothermal results (Figure 4.1), we find that the heating condition has not changed the data trend for these four stainless steel tubes. The friction factor results under all these three heating conditions have the same pattern and the same transition region start order for different tubes but the start and end Reynolds numbers changes (see Table 11).

The constricted flow parameters method proposed by Kandlikar et al. (2005) has been introduced in Chapter 3. From Figure 4.1 we can see that only the 560μm stainless steel tube friction factor in laminar region is higher than the theoretical value, so that we will apply this method to the current 560μm tube data only. For Nickel tubes, as they have an almost smooth inner surface, we would not apply this method to them. The 560μm stainless steel tube has a relative roughness of 2.95%. According to the constricted flow parameters method, the constricted diameter can be calculated by equation (2) and the constricted flow friction factor value can be calculated by equation (6). The results show that the difference between constricted flow friction factor and

conventional friction factor is 23%. That means the upward shift observed in the friction factor profile of the 560µm tube will be compensated by constricted flow parameters. This improvement was observed by Kandlikar et al. (2005) for micro channel with hydraulic diameter 953µm and relative roughness 7.3%. Similar observations were reported by Brackbill and Kandlikar (2007) for relative roughness ranging from 1.42% to 4.88% and hydraulic diameter ranging from 198µm to 1084µm. As Figure 4.10 shows, the observed laminar region constricted friction factor for the 560µm tube was not following the theoretical laminar line that means we need do more work in order to apply the constricted flow parameters method which works well on micro channels to micro tubes.

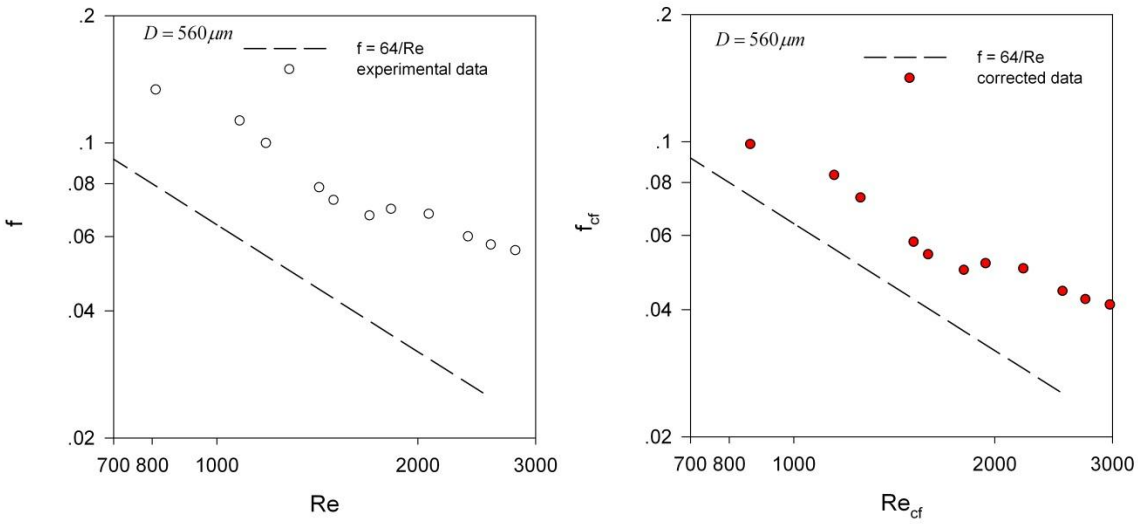

Figure 4.10 Friction factor for 560µm stainless steel tube (a) original data (b) data plotted with constricted parameters.

The isothermal run results from different researchers showed that the relative roughness of micro tubes inner surface can significantly affect the critical Reynolds number (Re_{cr}). According to the data obtained by Ghajar et al. (2010), Tam et al. (2011), and current test results; the relationship

between the critical Reynolds number and relative roughness (ε/D) can be plotted as shown in Figure 4.11.

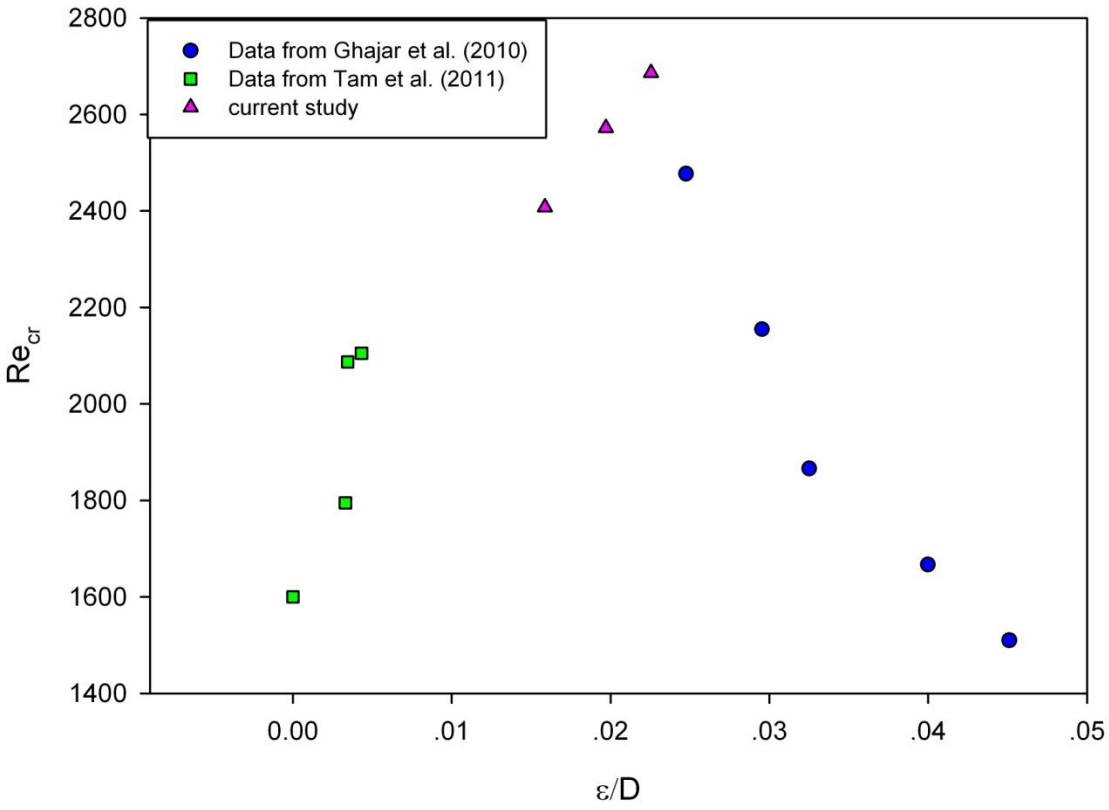

Figure 4.11 The critical Reynolds numbers of micro tubes for different relative roughness values

Figure 4.11 shows that when the micro tube relative roughness is zero (glass tubes), the critical Reynolds number is about 1600. The critical Reynolds number increases almost linearly to the higher value with the increase of relative roughness, and the critical Reynolds number reaches a maximum value (about 2700) when the relative roughness is about 0.025. After that the critical Reynolds number decreases to the smaller value. When the relative roughness is about 0.045 the critical Reynolds number goes back to 1500.

4.2 Heat Transfer Results

A series of correlations have been established in the literature for the normal size pipe. In this experiment the micro tubes experimental results will be compared with these correlations.

Gnielinski correlation (Gnielinski, 1976) for turbulent region:

$$Nu = [(f/8)(Re-1000)Pr]/[1.07+12.7(f/8)^{0.5}(Pr^{2/3}-1)] \quad (22)$$

$$f = \frac{4}{(3.64\log(\mathrm{Re})-3.28)^2} \quad (23)$$

Where $3000 \leqq Re \leqq 5000000$, $0.5 \leqq Pr \leqq 2000$.

Sieder and Tate correlation (Sider and Tate, 1936) for developing laminar region:

$$Nu = 1.86\left(\mathrm{Re}\,\mathrm{Pr}\frac{D}{L}\right)^{1/3}\left(\frac{\mu_b}{\mu_s}\right)^{0.14} \quad (24)$$

Where $0.6 \leqq Pr \leqq 5$, $0.0044 \leqq (\mu_b/\mu_s) \leqq 9.75$, $Re \leqq 2200$ and $(L/D)/(RePr) \leqq 0.05$.

Edwards correlation (Edwards et al., 1979) developing laminar region:

$$Nu = 7.54 + \frac{0.03(D_h/L)\,\mathrm{Re}^*\,\mathrm{Pr}}{1+0.016[(D_h/L)\,\mathrm{Re}\,\mathrm{Pr}]^{2/3}} \quad (25)$$

Where $Re \leqq 2800$ and $(L/D_h)/(RePr) \leqq 0.05$.

Ghajar and Tam correlation (Tam and Ghajar, 2006) for transition region:

$$Nu = Nu_l + \{\exp[(a-\mathrm{Re})/b] + Nu_t^c\}^c \quad (26)$$

For re-entrant inlet geometry (used in this experiment): $2700 \leqq Re \leqq 5500$, $16 \leqq Pr \leqq 35$, $7410 \leqq Gr \leqq 158300$ and $1.13 \leqq \mu_b/\mu_s \leqq 2.13$.

Where Nu_l = laminar flow Nusselt number, Nu_t = turbulent flow Nusselt number. a, b, c = Constants depending on inlet geometry. (Please refer to Tam and Ghajar (2006) for further details on experiments, expressions for Nu_l and Nu_t and values of constants.)

As the literature review shows that heat transfer test results from different researchers are different. Some of them obtained a higher value compared with conventional correlations. Some of them obtained a lower value. The resent experimental results show the heat transfer rate for micro tubes fit the conventional correlations well. It is reasonable that different researchers get different heat transfer results since the tubes that used by them are with different diameter and roughness. These kind of difference is mainly due to the tubes that tested by different researchers have different roughness and diameters. Kandlikar et al. (2003) found that the tubes with same diameter but different roughness have different heat transfer rate. In laminar region the heat transfer rate will increase with the increase of the roughness. Figure 4.12 shows the testing result for 0.62mm stainless steel tubes with different roughness. In this figure, "T_w mid" means the thermocouple location is in the middle of the testing tube.

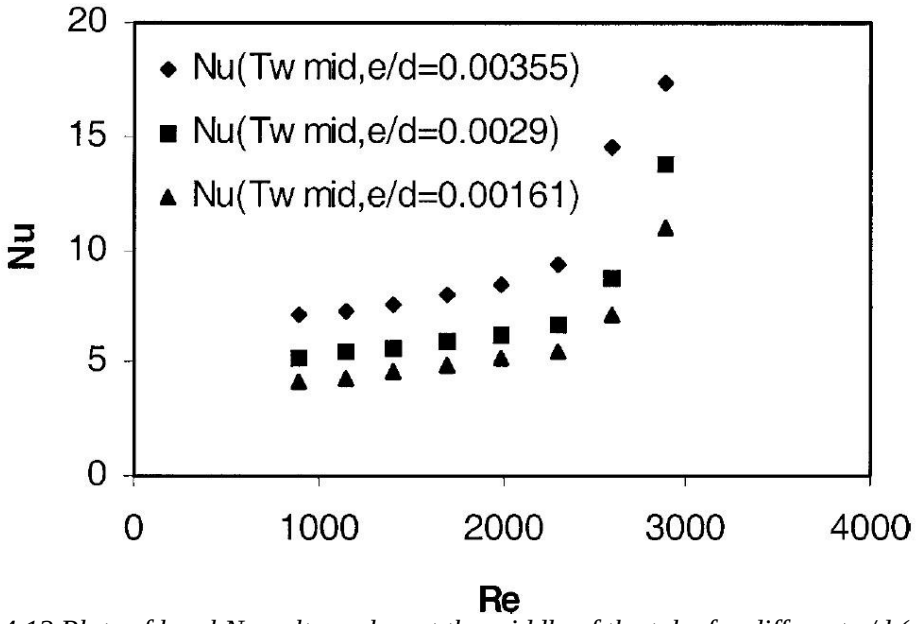

Figure 4.12 Plots of local Nusselt number at the middle of the tube for different e/d (relative roughness) ratio (0.62 mm dia. tube). [Kandlikar et al.(2003)]

Qi et al. (2007) conducted an experiment for single phase liquid Nitrogen flow in stainless steel micro tubes. According to the heat transfer rate results (Figure 4.12), the heat transfer rate in turbulent region is a little higher than the conventional theory and the heat transfer rate increases with diameter decrease.

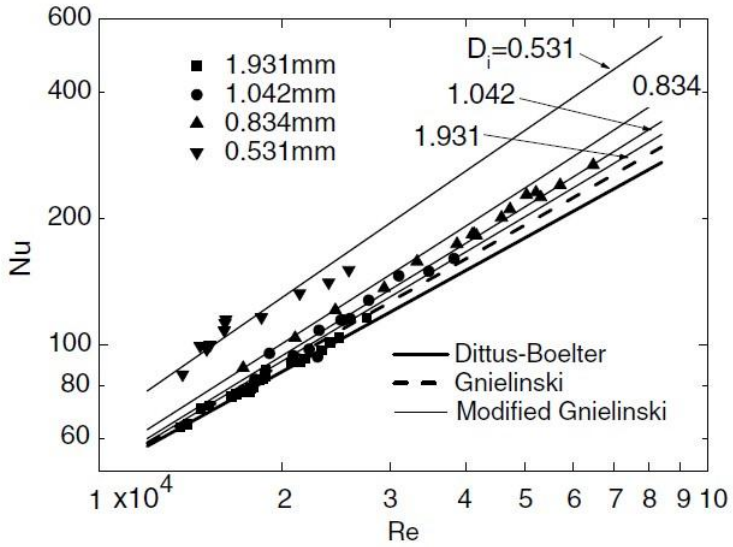

Figure 4.13 Comparison of the experimental Nusselt numbers of stainless steel tubes with the correlations for the conventional channels.[Qi et al.(2007)]

In the current study four stainless steel tubes and tree Nickel tubes have been tested. During the testing process, the testing tube was heated by electric current flow and the inlet and outlet temperature difference has been controlled to be 3°C by adjusting the electric current value. The heat balance in this experiment is the difference between the input DC power (Equation (1)) and the heat absorbed by water flow (Equation (15)). The heat balance error in this experiment is less than 3%, which means the testing tubes have been well insulated. The heat transfer results of stainless steel tubes have been plotted in Figure 4.14. The results show that, in laminar region the Nusselt numbers are slightly higher than the value predicted by Sieder and Tate correlation. In turbulent region the experimental Nusselt numbers fit the Gnielinski correlation well. In laminar

and turbulent regions the change in diameter has not affected the heat transfer rate. All four tubes' testing results are same.

In case of transition region, unlike friction factor, the Nusselt number was also not affected by the tube diameter in these stainless steel tubes. Figure 4.14 shows that the Nusselt number measured at the same Reynolds number did not change for all four stainless steel tubes. The Reynolds numbers at start and end of transition regions also stayed almost the same. Similar results have also been found by other researchers. As shown in Figure 4.15, Morini et al. (2010) preformed similar experiments. From their result, it is hard to say the tube diameter has any affect on heat transfer rate in the diameter range: from 440μm to 146μm. This kind of result can be explained by the relatively large roughness of the stainless steel tubes. The large roughness dominated the heat transfer in these tubes. The results also show us that for these stainless steel tubes, heat transfer is more sensitive to the roughness than the tube's diameter.

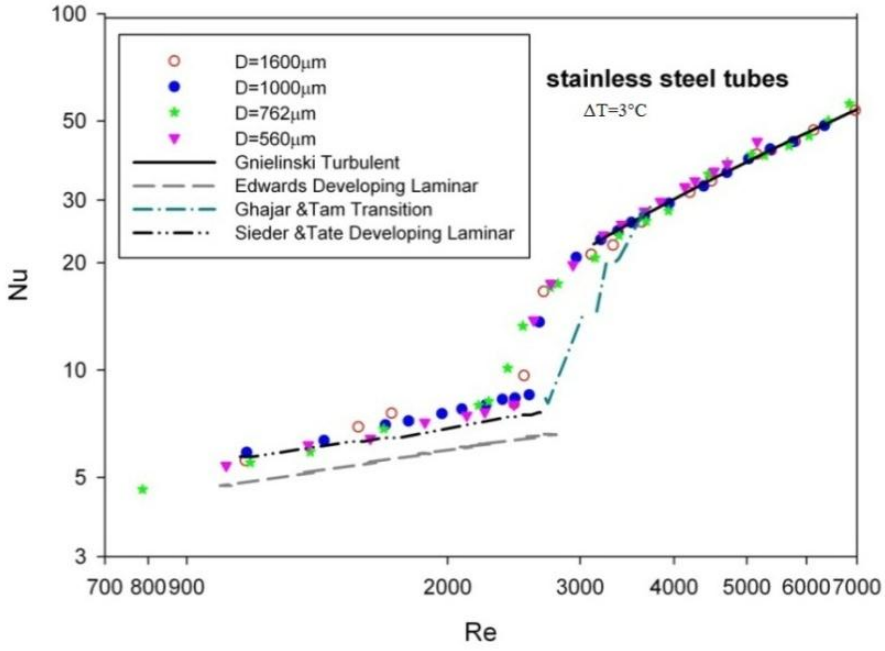

Figure 4.14 Nusselt number of four stainless steel tubes with diameter from 1600μm to 560μm.

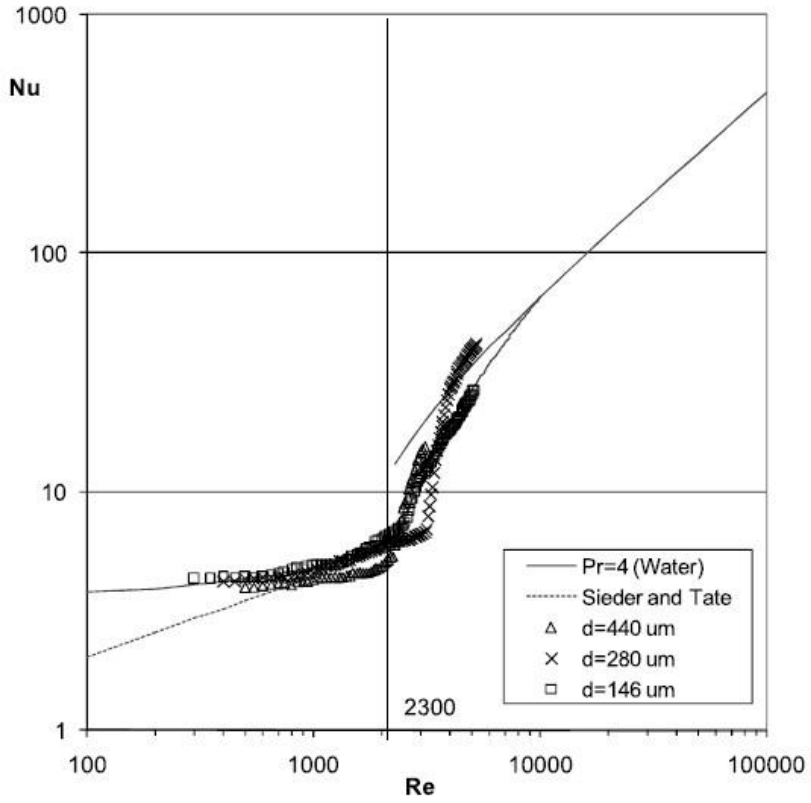

Figure 4.15 Average Nusselt numbers as a function of the Reynolds number for water flow through micro-tubes with: (a) d=146μm at ε/d=4.1%, (b) d= 280μm at ε/d=1.1%, and (c) d=440μm at ε/d=0.7%. [Morini et al. (2010).]

In order to more clearly figure out how the tube roughness and diameter affect the heat transfer rate, three nickel tubes have been tested. The only major difference of Nickel tube and stainless steel tube is that Nickel tube has a much smoother inner surface. As previous measurements showed the roughness of stainless steel tubes is about 16.5μm and the roughness for Nickel tubes is about 51nm which is more than 300 times smoother than stainless steel tubes (Table 8). The smooth inner surface will eliminate most of the roughness effect on heat transfer, so the diameter effect should be more clearly viewed. The results in Figure 4.16 show that the behavior of Nusselt number with respect to Reynolds number of these Nickel tubes is quite different than stainless steel tubes. In laminar and turbulent regions, the Nusselt number of Nickel tubes was about 15%

lower than that of stainless steel tubes. That's due to the relatively smooth inner surface of Nickel tubes. When the Nickel tube diameter decreased from 1016 µm to 500 µm, the Nusselt number in laminar region slightly reduced, but in the turbulent region the Nusselt number was not affected by the tube diameter. In the transition region heat transfer, the behavior of Nickel tubes has shown a strong relationship with the tube diameter. When the diameter of Nickel tube decreased from 1016 µm to 762 µm, the start Reynolds number of transition region shifted from 3207 to 3734 and the end Reynolds number also shifted from 3954 to 4860. When the tube diameter decreased from 762 µm to 508 µm, the start Reynolds number shifted back from 3734 to 3363, and the end Reynolds number shifted from 4860 to 4109. The plot also shows that the transition profile did not change when changing the diameter.

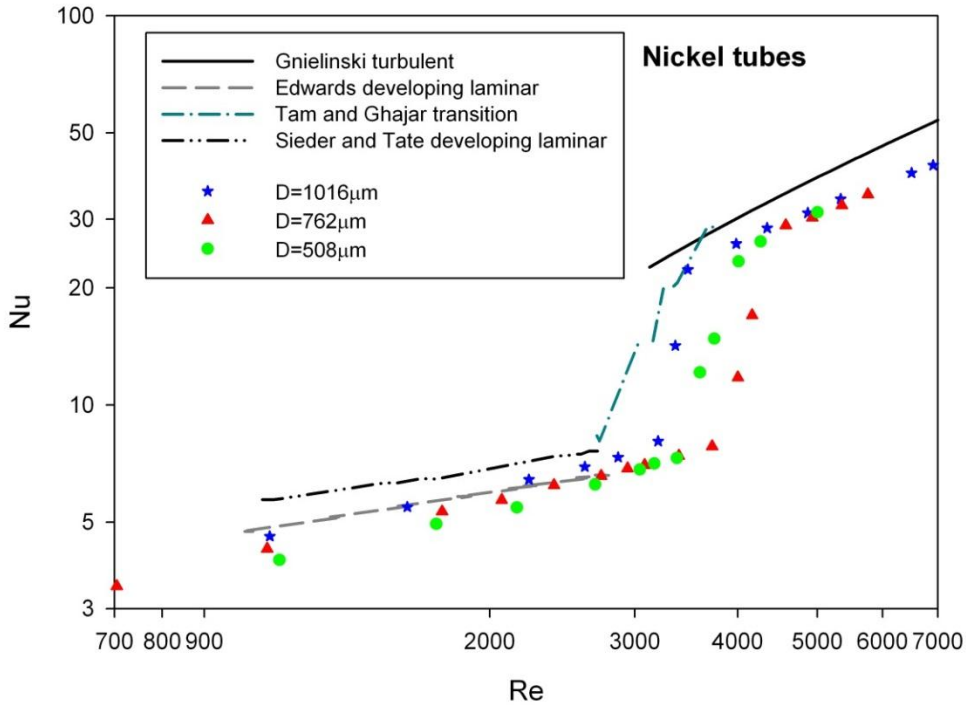

Figure 4.16 Nusselt number of three Nickel tubes with diameter 1016µm, 760µm and 500µm

The isothermal friction factor for the same Nickel tubes has been measured by Singh (2011). The results (Figure 4.17) showed that the 1016μm Nickel tube transition region started earlier than the 762μm. The 762μm Nickel tube transition region started later than the 562μm tube. This kind of transition region starting priority is the same with heat transfer. From Table 11, we can also see that for the same tube diameter, the transition region start Reynolds number of heat transfer is about 1000 larger than the transition region start Reynolds number of friction factor. That is due to the viscosity change under heating condition in heat transfer experiment. The same affect can be seen from the heating friction factor testament results for stainless steel tubes (Figure 4.4 to Figure 4.7).

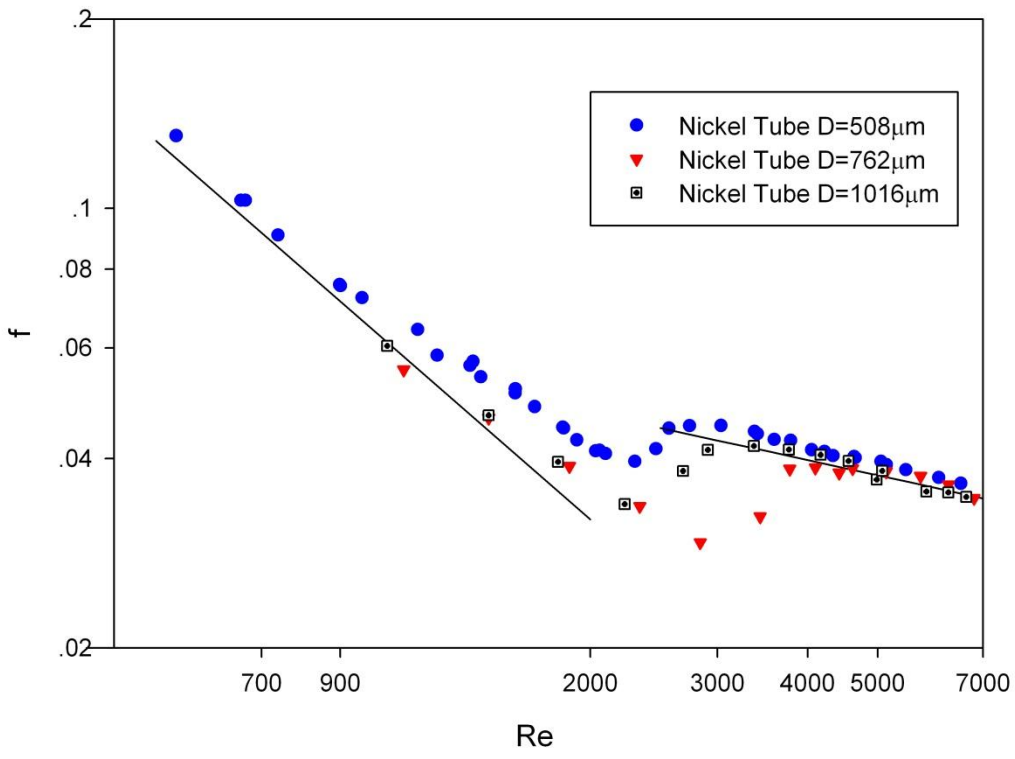

Figure 4.17 Friction factor of three Nickel tubes with diameter 508μm 762μm and 1016μm.[Singh (2011)]

CHAPTER V

CONCLUSIONS AND RECOMMEDATIONS

5.1 Conclusions

In this study, an experimental setup was designed and verified for the measurements of friction factor and heat transfer in horizontal micro-tubes under uniform wall heat flux boundary condition in all flow regimes (laminar-transition-turbulent).

The friction factor of four stainless steel tubes has been tested firstly. From the results the flowing conclusions can be drawn:

1) Under isothermal condition if the tube diameter decreased from 1600μm to 1000μm the start of transition region of friction factor shifted to the higher Reynolds numbers. When the tube diameter continually decreased to the small value (1000μm-560μm), the onset of transition from laminar flow occurred at lower Reynolds numbers.
2) Under constant heat flux condition the onset of transition region of the same tube has been delayed to higher Reynolds numbers by comparison with the isothermal condition.

The heat transfer test has been performed for four stainless steel tubes and three Nickel tubes. The stainless tubes' results did not show any tube diameter affect on the transition region. At the same time the heat transfer results from Nickel tubes which have a smoother inner surface have shown that the onset of transition region is affected by Nickel tube diameter. As the

only difference between Nickel tube and stainless steel tube is the inner surface roughness, we can conclude that: When the surface roughness is relatively large, the roughness will dominate the heat transfer rate. When the surface roughness value becomes relatively small, like Nickel tube, the tube diameter will show the affect on the heat transfer rate.

5.2 Recommendations

Current study has shown a promising direction for flow characteristics of micro tube research. However, more future work is needed in order to make a systematical conclusion about how the tube diameter and inner surface roughness effect the friction factor and heat transfer rate.

For friction factor, as only four stainless steel tubes with the same roughness have been tested, it is hard to tell the roughness affect on the friction factor. More tubes with the same diameter but different roughness need to be tested.

In case of heat transfer, the Nickel tubes' results verified the tube diameter will change the start and the end Reynolds numbers of transition region. Since only three Nickel tubes have been tested, we still cannot conclude how the heat transfer transition region changes with the changing of tube diameter. In order to figure out this relationship, more Nickel tubes with different diameter should be tested.

REFERENCES

Asako, Y., Nakayama, K., Shinozuka, T., "Effect of Compressibility on Gaseous Flows in a Micro-tube," *International Journal of Heat and Mass Transfer,* Vol. 48, pp.4985-4994, 2005.

Aydin.O., and Avci.M., "Analysis of Laminar Heat Transfer in Mirco-poiseuille flow," *International Journal of Thermal Science,* Vol. 46, pp. 30-37, 2006.

Brackbill, T. P., and Kandlikar, S. G., "Effects of Low Uniform Relative Roughness on Single Phase Friction Factors in Microchannels and Minichannels."*International Conference on Nanochannels, Microchannels and Minichannels* .Puebla, Mexico, 2007.

Brutin, D., Tadrist, L., "Experimental Friction Factor of a Liquid Flow in Micro-tubes," *Physics of Fluids*, vol. 15, pp.653-661, 2003.

Celata, P. G., Cumo, M., Guglielmi, M. and Zummo, G., "Experimental Investigation of Hydraulic and Single-phase Heat Transfer in 0.130-mm Capillary Tube," *MicroscaleThermophysical Engineering*, Vol. 6, pp. 85-97, 2002.

Celeta, G.P., Cumo, M., McPhail, S., and Zummo, G., "Characterization of Fluid Dynamic Behavior and Channel Wall Effects in Microtube," *International Journal of Heat and Fluid Flow,* Vol. 27, pp. 135-143, 2006a.

Celeta, G.P., Cumo, M., McPhail, S.J., Tesfagabir, L., Zummo, G., "Experimental Study on Compressible Flow in Micro-tubes," *International Journal of Heat and Mass Transfer*, Vol. 28, pp. 28-36, 2006b.

Celata, P. G., Cumo, M., Marconi, V., Mcphail, S. J. and Zumo, G., "Microtube Liquid Single-Phase Heat Transfer in Laminar Flow," *International Journal of Heat and Mass Transfer*, Vol. 49, pp. 3538-3546, 2006c.

Cook, L. W., "A Experimental Apparatus for Measurement of Pressure Drop, Void Fraction, and Non-boiling Two-phase Heat Transfer and Flow Visualization in Pipes for All Inclinations." MS thesis, Oklahoma State University, 2008.

Cui, H. H., Silber-Li, Z.H., Zhu, S.N., "Flow Characteristics of Liquids in Micro-tubes Driven by a High Pressure."Physics of Fluids, vol. 16, pp. 1803-1810, 2004.

Edwards, D. K., Denny, V. E., Mills, A. F., *Transfer Processes*. 2nd ed. Washington, DC: Hemisphere, 1979.

Ghajar, A. J., Tang, C. C., and Cook, W. L., "Experimental Investigation of Friction Factor in the Transition Region for Water Flow in Minitubes and Microtubes." *Heat Transfer Engineering*, Vol. 31, No. 8, pp. 646-657, 2010.

Ghajar, A. J., and Kim, J., "Calculation of Local Inside-Wall Convective Heat Transfer Parameters from Measurements of the Local Outside-Wall Temperatures along an Electrically Heated Circular Tube," in *Heat Transfer Calculations*, edited by Myer Kutz, McGraw-Hill, New York, NY, pp. 23.3-23.27, 2006.

Gnielinski, V., "New Equations for Heat and Mass Transfer in Turbulent Pipe and Channel Flow," *International Chemical Engineering*, Vol. 16, pp. 359 – 368, 1976

Grohmann, H., "Measurement and Modeling of Single-Phase and Flow-Boiling Heat Transfer in Micro-tubes," *International Journal of Heat and Mass Transfer*, Vol. 48, pp. 4073-4089, 2005.

Hrnjak, P., Tu, X., “Single Phase Pressure Drop in Microchannels,” *International Journal of Heat and Fluid Flow,* Vol.28, pp. 2-14, 2007.

Hu, J. S. and Chao, C. Y. H., “An Experimental Study of the Fluid Flow and Heat Transfer Characteristics in Micro-condensers with Slug-bubbly Flow,” *International Journal of Refrigeration*, Vol. 30, pp. 1309-1318, 2007.

Hwang, Y.W., Kim, M.S., “The Pressure Drop in Micro-tubes and the Correlation Development,” *International Journal of Heat and Mass Transfer*, Vol. 49, pp.1804-1812, 2006.

Kandlikar, S. G., Joshi. S., and Tian, S. R., "Effect of Surface Roughness on Heat Transfer and Fluid Flow Characteristics at Low Reynolds Numbers in Small Diameter Tubes." *Heat Transfer Engineering,*Vol.24, pp. 4-16, 2003.

Kandlikar, S. G., Schmitt, D., Carrano, A. L., Taylor, J. B. "Characterization of Surface Roughness Effects on Pressure Drop in Single Phase Flow in Minichannels." *Physics of Fluids*, Vol.10,pp. 100606, 2005.

Kline, S. J., McClintock, F. A., “Describing Uncertanities in Single-sample Experiments.” *Mechanical Engineering Vol.*75, pp.3-8, 1953.

Li, Z.X., Du, D.X., Guo, Z.Y., “Experimental study on flow characteristics of liquid in circular micro-tubes,” *Microscale Thermophysical Engineering*, Vol.7, pp.253-265, 2003.

Li, Zhuo., He, Y. L., Tang. G. H., and Tao. W. Q., "Experimental and Numerical Studies of Liquid Flow and Heat Transfer in Microtubes." *International Journal of Heat and Mass Transfer* Vol. 50, pp. 3447-60, 2007.

Liu, Z. G., Liang, S. Q. and Takei, M., "Experimental Study on Forced Convective Heat Transfer Characteristics in Quartz Micro-Tube," *International Journal of Thermal Science*, Vol.48, pp. 139-148, 2007.

Mala, G.M., Li, D.Q., "Flow Characteristics of Water in Micro-tubes,"*International Journal of Heat and Fluid Flow,* Vol. 20, pp. 142-148, 1999.

Morini, G.L., Lorenzini, M., Salvigni, S., "Friction Characteristics of Compressible Gas Flow in Micro-tubes" *Experimental Thermal and Fluid Science,* Vol. 30, pp. 733-744, 2006.

Morini, G. L., Lorenzini, M., Salvigni, S., Celata, G. P.,"Experimental Analysis of Microconvective Heat Transfer in the Laminar and Transitional Regions,"*Experimental Heat Transfer*, Vol. *23*, pp. 73-93, 2010.

Muwanga, R., and Hassan, I., "Local Heat Transfer Measurement in Microchannels Using Liquid Crystal Thermography: Methodology Development and Validation," ASME Journal of Heat Transfer, Vol. 128, pp. 617-626, 2006.

Owhaib, W. and Palm, B., "Experimental Investigation of single-phase convective heat transfer in circular micro channel," *Experimental Thermal and Fluid Science*, Vol. 28, pp. 105-110, 2004.

Qi, S. L., Zhang, P., Wang, R. Z. and Xu, L. X., "Single-phase Pressure Drop and Heat Transfer Characteristics of Turbulent Liquid Nitrogen Flow in Micro-tubes," *International Journal of Heat and Mass Transfer,* Vol. 50, pp. 1993-2001, 2007.

Qu, W., Mudawar, I., "Experimental and Numerical Study of Pressure Drop and Heat Transfer in a Single-phase Micro-channel Heat sink," *International Journal of Heat and Mass Transfer* , Vol.45, pp. 2549-2565, 2002.

Rands, C., Webb, B.W. and Maynes, D., "Characterization of Transition to Turbulence in Microchannels," *International Journal of Heat and Mass Transfer,* Vol. 49, pp. 2924-2930, 2006.

Shen, S., Xu, J. L., Zhou, J. J. and Chen, Y., "Flow and Heat Transfer in Microchannels with Rough Wall Surface", *Energy Conversion and Management,* Vol. 47, pp. 1311-1325, 2005.

Sieder, E. N. and Tate, G. E., "Heat Transfer and Pressure Drop of Liquids in Tubes," *Industrial and Engineering Chemistry*, Vol. 28, No. 12, pp. 1429 – 1435, 1936.

Singh, A., "Experimental Investigation of Friction Factor in Microtubes and Development of Correlations for Prediction of Critical Reynolds Number." MS thesis, Oklahoma State University, 2011.

Steinke, M.E., Kandilikar, S.G., "Single-phase Liquid Friction Factors in Microchannels," *International Journey of Thermal Sciences,* Vol. 45, pp. 1073-1083, 2006.

Tam, L. M. and Ghajar, A. J, "Transitional Heat Transfer in Plain Horizontal Tubes," *Heat Transfer Engineering*, Vol. 27, pp. 23-38, 2006.

Tam, L. M., Ghajar, A. J., and Tam, H. K., "Contribution Analysis of Dimensionless Variables for Laminar and Turbulent Flow Convection Heat Transfer in Horizontal Tube Using Artificial Neural Network", *Heat Transfer Engineering*, Vol. 29(9), pp. 793-804, 2008.

Tam, L. M., Tam, H. K., Ghajar, A. J., Ng, W. S., "Heat Transfer Measurements for a Horizontal Micro-Tube Using Liquid Crystal Thermography," *Proceedings of the 4th International Symposium on Heat Transfer and Energy Conservation (ISHTEC2012),* Guangzhou, China, January 6-9, 2012.

Tam, H. K., Tam, L. M., Ghajar, A. J., Ng, W. S., Wong, I. W., Leong, K. F., and Wu, C. K., "The Effect of Inner Surface Roughness and Heating on Friction Factor in Horizontal Micro-Tubes", *ASME-JSME-KSME Joint Fluids Engineering Conference,* Japan, 2011.

Yang, C. Y., and Lin, T. Y., "Heat Transfer Characteristics of Water Flow in Micro-tubes," *Experimental Thermal and Fluid Science*, Vol. 32, pp. 432-439, 2007.

Young, P. L., Brackbill, T. P., and Kandlikar, S. G., "Estimating Roughness Parameters Resulting from Various Machining Techniquesfor Fluid Flow Applications," Heat *Transfer Engineering*,vol. 30, no. 1–2, pp. 78–90, 2009.

Yin, J.M., Bullard, C.W., Hrnjak, P.S., "Single-phase Pressure Drop Measurements in a Microchannel Heat Exchanger," *Heat Transfer Engineering*, 23: 3-12, 2002.

Zhigang, Liu.,Ning, G, and Takei, M., "An Experimental Investigation of Single-Phase Heat Transfer in 0.045mm to 0.141mm Microtubes," *Nanoscale and MicroscaleThermophysical Engineering* 11: 3-4,2007.

Qian Li

Candidate for the Degree of

Master of Science

Thesis: EXPERIMENTAL INVESTIGATION OF FRICTION FACTOR AND HEAT TRANSFER FOR SINGLE PHASE WATER FLOW IN STAINLESS STEEL AND NICKEL MICRO-TUBES

Major Field: Mechanical and Aerospace Engineering

Biographical:

Education:

Completed the requirements for the Master of Scince in Mechanical and Aerospace Engineering at Oklahoma State University, Stillwater, Oklahoma in July, 2012.

Completed the requirements for the Bachelor of Science in Electromechanical Engineering at University of Macau, Macau, China in 2010.

Experience: School of Mechanical and Aerospace Engineering as a teaching assistant. Oklahoma State University School of Mechanical and Aerospace Engineering, 2010 to 2012.

Name: Qian Li Date of Degree: July, 2012

Institution: Oklahoma State University Location: Stillwater, Oklahoma

Title of Study: EXPERIMENTAL INVESTIGATION OF FRICTION FACTOR AND HEAT TRANSFER FOR SINGLE PHASE WATER FLOW IN STAINLESS STEEL AND NICKEL MICRO-TUBES

Pages in Study: 76 Candidate for the Degree of Master of Science

Major Field: Mechanical and Aerospace Engineering

Scope and Method of Study: This study has been conducted in order to present the design, construction and validation of a state-of-the-art experimental apparatus for the purpose of measuring pressure drop and heat transfer in micro-tubes. The data collected by this method has been compared with the previous research work and established conventional correlations for friction factor and heat transfer. All the data also have been analyzed by different flow regions (laminar-transition-turbulent).

Findings and Conclusions: The inner surface roughness and diameter play significant roles in friction factor and heat transfer of micro-tubes. A change in relative roughness of micro-tubes causes a change in the transition region of friction factor. The start and the end Reynolds numbers of transition region shift to the higher value when the stainless steel tubes diameter reduced from 1600μm to 1000μm. From 1000μm to 560μm, the start and the end Reynolds numbers of transition region for these stainless steel tubes become smaller with the decrease of diameter. For heat transfer, the large roughness dominates the heat transfer rate in stainless steel tubes. In very smooth nickel tubes, tube diameter has an effect on the heat transfer rate in the transition region. When the nickel tube diameter decreased from 1016μm to 762μm, the start of transition region of heat transfer shifted from 3207 to 3734. When the nickel tube diameter decreased to 508μm, the start Reynolds number of transition region shifted back to 3363 from 3734.

ADVISER'S APPROVAL: Dr. Afshin J. Ghajar